Supporting Information

Crystal engineering of a family of hybrid ultramicroporous materials based upon interpenetration and dichromate linkers

Hayley S. Scott,[a] Naoki Ogiwara,[b] Kai-Jie Chen,[a] David G. Madden,[a] Tony Pham,[c] Katherine Forrest,[c] Brian Space,[c] Satoshi Horike,[b] John J. Perry IV,[a] Susumu Kitagawa[b,d*] and Michael J. Zaworotko*[,a]

[a] Bernal Institute, Department of Chemical and Environmental Science, University of Limerick, Republic of Ireland

[b] Department of Synthetic Chemistry and Biological Chemistry, Kyoto University, Katsura, Nishikyo-ku, Kyoto, 615-8510, Japan

[c] Department of Chemistry, University of South Florida, 4202 East Fowler Avenue, Tampa, Florida, 33620, U.S.A

[d] Institute for Integrated Cell-Material Sciences (iCeMS), Kyoto University, Yoshida, Sakyo-ku, Kyoto 606-8501, Japan

Table of Contents

General

All reagents and solvents were purchased from Sigma-Aldrich and used as received. Fourier Transform Infrared (FT-IR) spectra were measured on a Perkin Elmer Spectrum 100 spectrometer with Universal ATR accessory between the range of 4000-650 cm^{-1}. Powder X-ray diffraction measurements were performed on a Rigaku RINT 2200 Ultima diffractometer with Cu-K_α anode. Patterns were collected from 3° to 40° 2θ, using a step size of 0.02° at a scan rate of 0.1 °/min. Thermogravimetric analyses (TGA) were performed using a Rigaku TG8120, under flowing N_2 between the temperature range 25-500 °C with 10 °C/min ramp rate. Gas sorption isotherms were measured using BELSORP-mini equipment. Water sorption isotherms were measured using BELSORP-aqua equipment. X-ray crystallographic measurements for **DICRO-3-Cu-i** were collected at 100(2) K, under N_2 flow, on a Bruker Quest D8 Mo Sealed Tube equipped with CMOS camera and Oxford cryosystem (λ = 0.71073 Å). The data collection and integration were performed within SMART and SAINT+ software programs,[1] and corrected for absorption using the multi-scan method implemented in SADABS.[2] X-ray crystallographic measurements on **DICRO-3-Co-i, DICRO-3-Ni-i** and **DICRO-3-Zn-i** were performed at 150(2), 173(2) and 173(2) K, respectively under N_2 flow, on a Rigaku AFC10 diffractometer with Rigaku Saturn Kappa CCD system equipped with a MicroMax-007 HF/VariMax rotating-anode X-ray generator with confocal monochromated Mo-K_α radiation (λ = 0.71073 Å). Data collection and integration were performed by CrystalClear 1.4.0, d*TREK.[3] Crystallographic data and refinement parameters for all compounds, given in Table S1, were solved by direct methods (SHELXS-97), and refined (SHELXL-97) by full least-squares on all F^2 data.[4] All non-hydrogen atoms were refined anisotropically and all framework hydrogen atoms were placed in calculated positions. Crystals of **DICRO-3-Co-i** were very small (0.03 × 0.03 × 0.03 mm) and weakly diffracting. As such, even after multiple collections on separate batches of sample, structural quality for this compound remains low. The overall structure, unit cell and space group of **DICRO-3-Co-i**, however, follows that of the three other compounds in the series. The contribution of the disordered solvent molecules was subtracted from the reflection data for all structures by the SQUEEZE method as implanted in the program PLATON.[4b]

Syntheses

Syntheses of single crystals:

DICRO-3-Co-i

$Co(NO_3)_2 \cdot 6H_2O$ (10 mg, 0.034 mmol), 4,4′-azopyridine (12.5 mg, 0.068 mmol) and $K_2Cr_2O_7$ (10 mg, 0.034 mmol) were dissolved in 2 mL H_2O and placed and in a 4 mL capacity vial that was then sealed. The vial and contents were heated to 120 °C for 48 h and cooled slowly to 30 °C over a 6 hour period. Upon cooling, small dark red-coloured crystals had formed on the sides of the vial. MW 697.36; Yield 9 mg (37%).

DICRO-3-Cu-i

$Cu(NO_3)_2 \cdot 3H_2O$ (13 mg, 0.05 mmol) and $K_2Cr_2O_7$ (15 mg, 0.05 mmol) were dissolved in 2 mL H_2O. Separately, 4,4′-azopyrdine (20 mg, 0.10 mmol) was dissolved in 2 mL MeCN. In a long, thin test tube the aqueous $Cu^{2+}/Cr_2O_7^{2-}$ solution was placed. Carefully layered on top of that was a 2 mL solution of H_2O:MeCN (1:1/v:v). The MeCN ligand solution was then carefully layered upon the H_2O:MeCN layer and the test tube sealed and left to sit. Crystals of X-ray diffraction quality had formed after one week. MW 719.99; Yield 20 mg (55%).

DICRO-3-Ni-i

The synthesis for this compound follows that of **DICRO-3-Cu-i**, however $Ni(NO_3)_2 \cdot 6H_2O$ (14 mg, 0.05 mmol) was used in place of $Cu(NO_3)_2 \cdot 3H_2O$. MW 715.14; Yield 11 mg (54%).

DICRO-3-Zn-i

The synthesis for this compound follows that of **DICRO-3-Cu-i**, however $Zn(NO_3)_2 \cdot 6H_2O$ (14 mg, 0.05 mmol) was used in place of $Cu(NO_3)_2 \cdot 3H_2O$. MW 703.82; Yield 22 mg (62%).

Syntheses of bulk powder products of DICRO-3-M-i:

$K_2Cr_2O_7$ (294 mg, 1.0 mmol) and $M(NO_3)_2 \cdot xH_2O$ ((1.0 mmol, ($Co(NO_3)_2 \cdot 6H_2O$ = 291 mg, $Ni(NO_3)_2 \cdot 6H_2O$ = 291 mg, $Cu(NO_3)_2 \cdot 3H_2O$ = 241 mg, $Zn(NO_3)_2 \cdot 6H_2O$ =

297 mg)) were dissolved in 20 mL of H_2O and stirred at room temperature. Separately, 4,4′-azopyridine (368 mg, 2.0 mmol) was dissolved in 20 mL of MeCN. To the stirring aqueous solution of $M(NO_3)_2$ and $K_2Cr_2O_7$, the 4,4′-azopyridine solution in MeCN was added drop-wise, to form an immediate precipitate. The product was left stirring overnight, after which time it was removed from stirring and the mother liquor exchanged with fresh MeCN twice a day until the solution became clear.

For activation, **DICRO-3-Co-i** and **DICRO-3-Ni-i** were placed under reduced pressure (0.0030 mmHg) at heated to 100 °C for 12 h, while **DICRO-3-Cu-i** and **DICRO-3-Zn-i** were placed under reduced pressure (0.0030 mmHg) at ambient temperature for 12 h.

Powder X-ray diffraction data

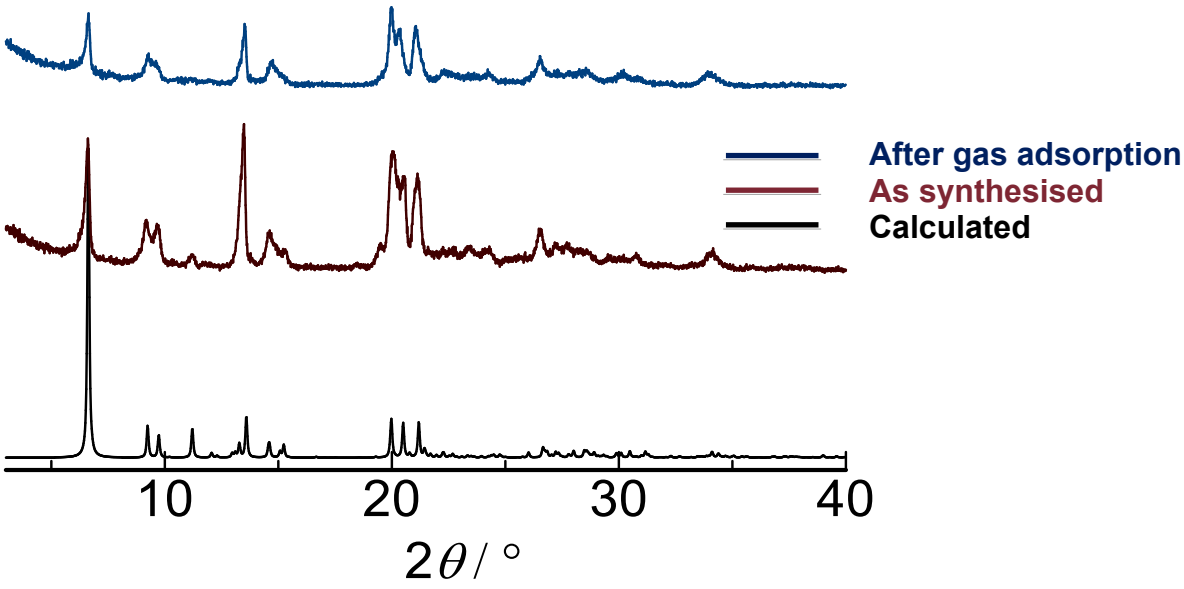
After gas adsorption
As synthesised
Calculated
10
20
30
40
2θ / °

Figure S1. PXRD diffractograms of **DICRO-3-Co-i**.

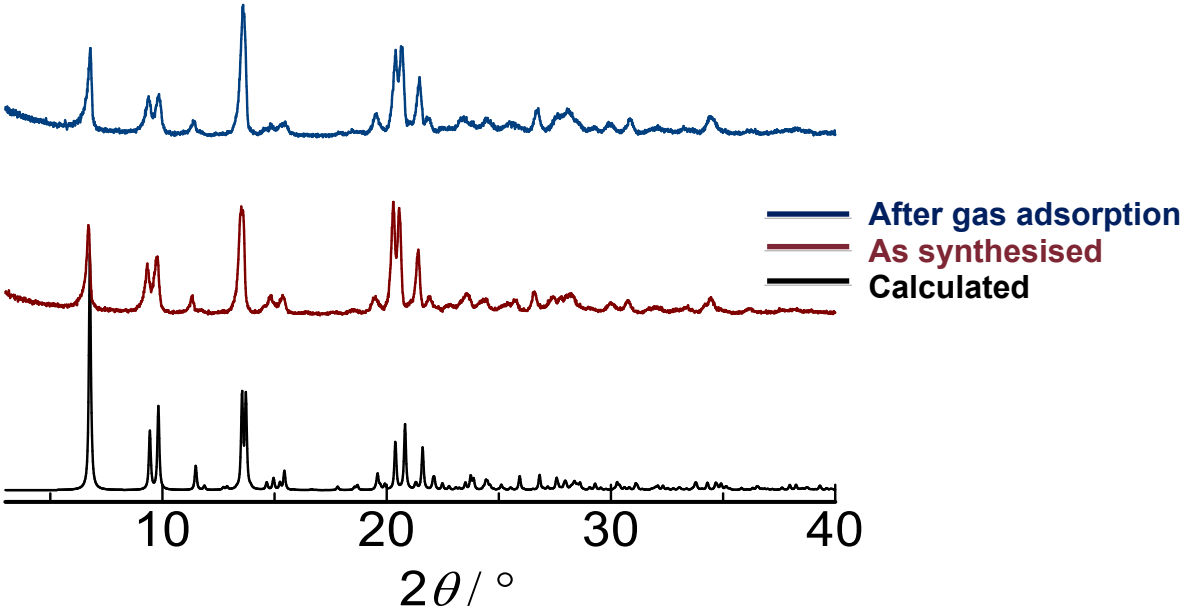
After gas adsorption
As synthesised
Calculated
10
20
30
40
2θ / °

Figure S2. PXRD diffractograms of **DICRO-3-Ni-i**.

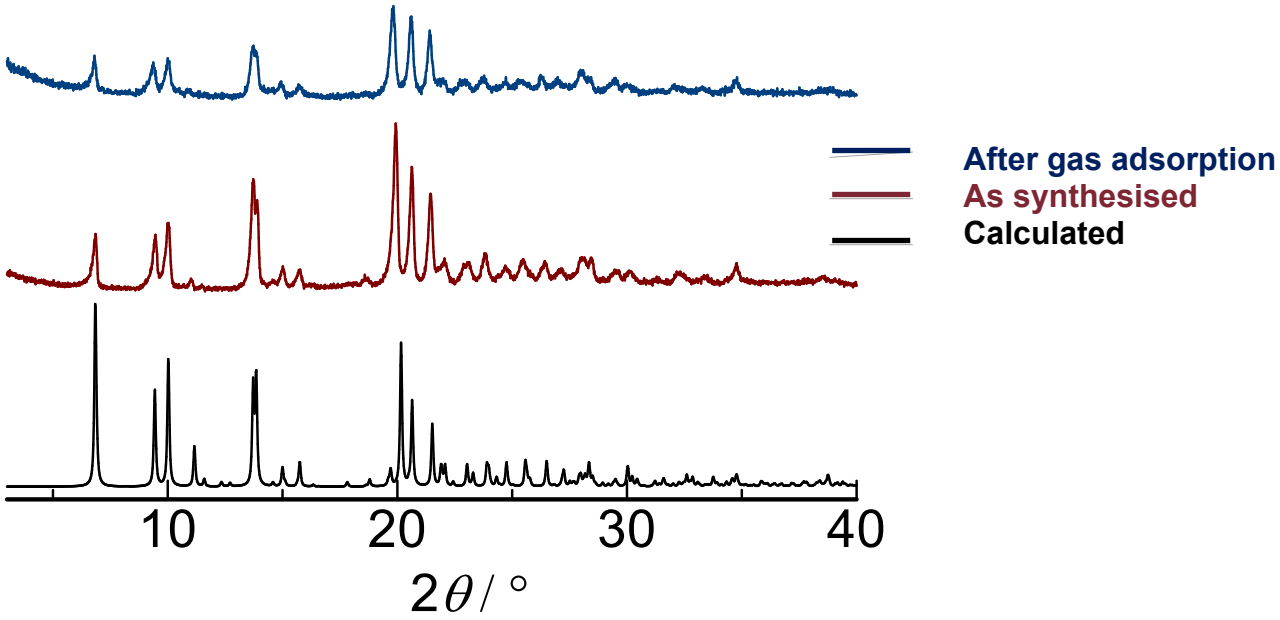
After gas adsorption
As synthesised
Calculated
10
20
30
40
2θ / °

Figure S3. PXRD diffractograms of **DICRO-3-Cu-i**.

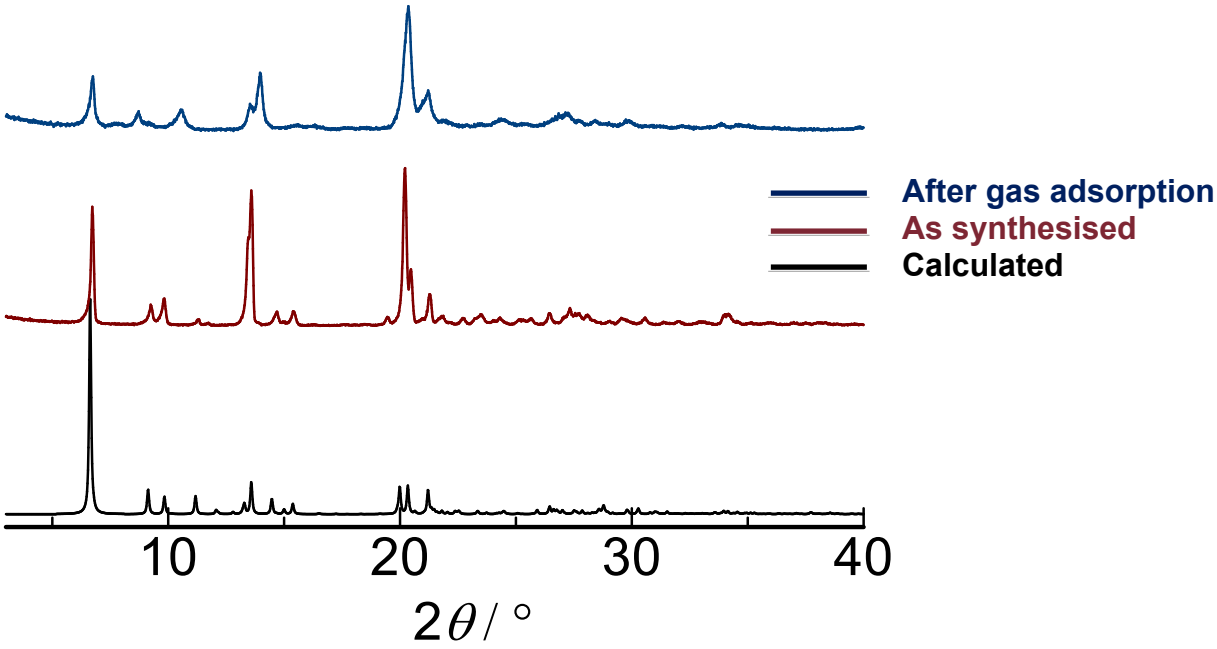
After gas adsorption
As synthesised
Calculated
10
20
30
40
2θ / °

Figure S4. PXRD diffractograms of **DICRO-3-Zn-i**.

Thermogravimetric analyses

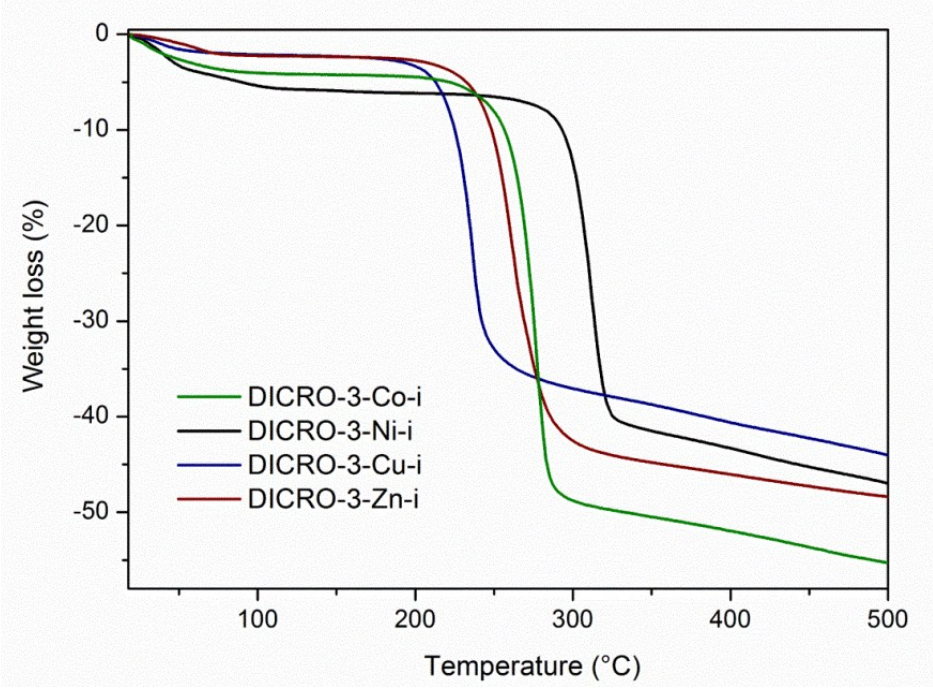

Figure S5. TGA measurements of **DICRO-3-M-i**.

Infrared spectra

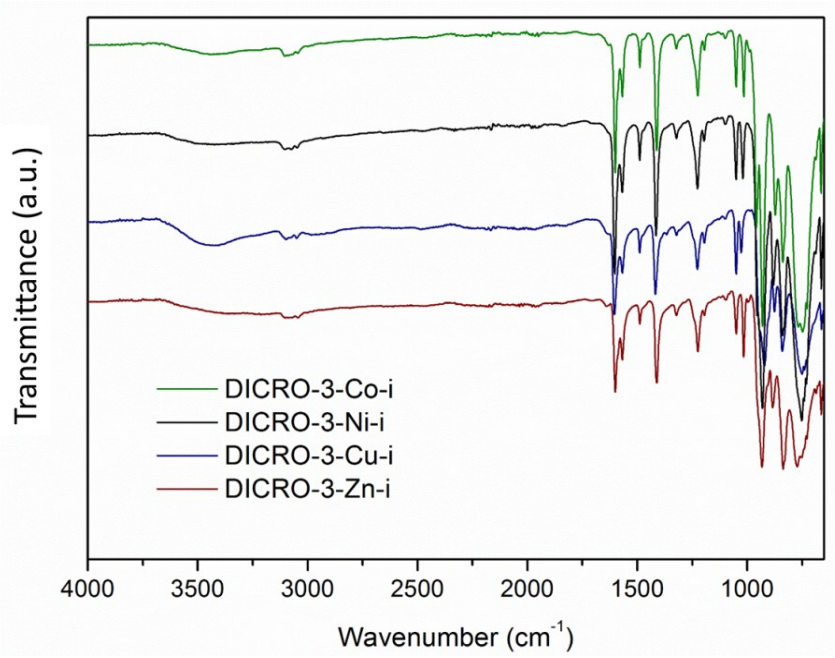

Figure S6. Infrared spectra of **DICRO-3-M-i**.

Single crystal diffraction data

Table S1. Crystal data and refinement details.

Compound	DICRO-3-Co-i	DICRO-3-Ni-i	DICRO-3-Cu-i	DICRO-3-Zn-i
Formula	$C_{20}H_{16}N_8O_7Cr_2Co_1$	$C_{20}H_{16}N_8O_7Cr_2Ni_1$	$C_{20}H_{16}N_8O_7Cr_2Cu_1$	$C_{20}H_{16}N_8O_{10}Cr_2Zn_1$
MW (g/mol)	643.34	643.12	647.95	649.78
T (K)	150	173	100	173
Crystal system	Triclinic	Triclinic	Triclinic	Triclinic
Space group	*P*-1	*P*-1	*P*-1	*P*-1
Z	2	2	2	2
a (Å)	8.799(6)	8.7338(17)	8.9931(11)	8.7822(18)
b (Å)	13.246(9)	13.153(3)	13.0017(16)	13.270(3)
c (Å)	13.340(8)	13.155(3)	13.0138(16)	13.278(3)
α (°)	87.784(17)	86.75(3)	85.457(3)	85.51(3)
β (°)	89.283(14)	84.55(3)	79.543(3)	80.23(3)
γ (°)	79.794(18)	80.39(3)	83.613(3)	83.94(3)
V (Å^3)	1528.1(17)	1481.9(3)	1484.4(3)	1513.6(5)
ρ_{calc} (g/cm^{-3})	1.398	1.441	1.450	1.426
μ (mm^{-1})	1.282	1.397	1.477	1.539
Measured/independent Reflections (R_{int})	19295/6559(0.0918)	18023/6746(0.0370)	28759/6097(0.0813)	18101/6889(0.0261)
Observed reflections [I > 2σ(I)]	4927	5763	4004	6171
R_1[a], wR_2[b] [I > 2σ(I)]	0.1580, 0.3935	0.0612, 0.1537	0.0632, 0.1243	0.0425, 0.1086
R_1, wR_2 (all data)	0.1756, 0.4030	0.0716, 0.1614	0.1107, 0.1375	0.0471, 0.1121
Goodness-of-fit on F^2	1.586	1.057	1.018	1.060

Table S2. Selected bond lengths and angles for **DICRO-3-M-i** compounds.

	DICRO-3-Co-i	DICRO-3-Ni-i	DICRO-3-Cu-i	DICRO-3-Zn-i
Lengths (Å)				
N(1)-M(1)	2.162(7)	2.108(3)	2.036(5)	2.160(3)
N(4)-M(1)	2.151(8)	2.101(3)	2.048(5)	2.138(3)
N(5)-M(1)	2.142(9)	2.068(4)	2.020(5)	2.161(2)
N(8)-M(1)	2.195(10)	2.087(4)	2.019(5)	2.177(2)
O(1)-M(1)	2.012(7)	2.046(3)	2.274(4)	2.088(2)
O(7)-M(1)	2.026(7)	2.033(3)	2.342(4)	2.111(2)
Cr(1)-O(1)	1.644(7)	1.628(3)	1.618(4)	1.635(2)
Cr(1)-O(2)	1.603(10)	1.588(5)	1.603(4)	1.598(3)
Cr(1)-O(3)	1.562(10)	1.592(5)	1.622(5)	1.609(3)
Cr(1)-O(4)	1.767(7)	1.778(4)	1.784(5)	1.775(3)
Cr(2)-O(4)	1.772(7)	1.778(4)	1.786(5)	1.782(3)
Cr(2)-O(5)	1.597(9)	1.595(4)	1.601(6)	1.593(4)
Cr(2)-O(6)	1.592(9)	1.611(4)	1.609(5)	1.587(4)
Cr(2)-O(7)	1.627(7)	1.636(3)	1.615(4)	1.632(2)
Angles (°)				
O(1)-M-O(7)	178.1(3)	177.78(13)	175.40(15)	178.24(10)
O(1)-M-N(5)	90.0(3)	89.54(15)	93.60(17)	90.03(9)
O(7)-M-N(5)	88.1(3)	88.56(14)	90.96(18)	89.38(10)
O(1)-M-N(4)	88.5(3)	88.88(13)	90.20(17)	88.69(10)
O(7)-M-N(4)	91.4(3)	90.02(13)	90.55(17)	89.68(11)
N(5)-M-N(4)	92.0(3)	91.66(14)	87.56(19)	92.19(10)
O(1)-M-N(1)	91.6(3)	91.77(13)	89.51(17)	91.67(11)
O(7)-M-N(1)	88.6(3)	89.43(13)	89.91(17)	89.98(11)
N(5)-M-N(1)	91.5(3)	91.27(14)	90.23(19)	89.48(10)
N(4)-M-N(1)	176.5(3)	177.00(14)	177.76(19)	178.29(10)
O(1)-M-N(8)	91.4(3)	90.18(15)	87.07(17)	89.41(9)
O(7)-M-N(8)	90.5(3)	91.75(14)	88.38(18)	91.29(10)
N(5)-M-N(8)	178.5(3)	178.65(13)	178.7(2)	175.94(10)
N(4)-M-N(8)	88.6(3)	89.66(14)	91.34(19)	91.82(10)
N(1)-M-N(8)	88.0(3)	87.42(14)	90.87(19)	86.52(10)
M-O(1)-Cr(1)	154.9(5)	158.7(2)	167.0(2)	163.25(14)
O(1)-Cr(1)-O(4)	109.2(4)	108.86(17)	108.8(2)	109.52(12)
O(4)-Cr(2)-O(7)	110.1(4)	109.53(17)	107.6(2)	108.95(13)
Cr(1)-O(4)-Cr(2)	135.6(5)	126.0(2)	127.3(3)	126.06(16)

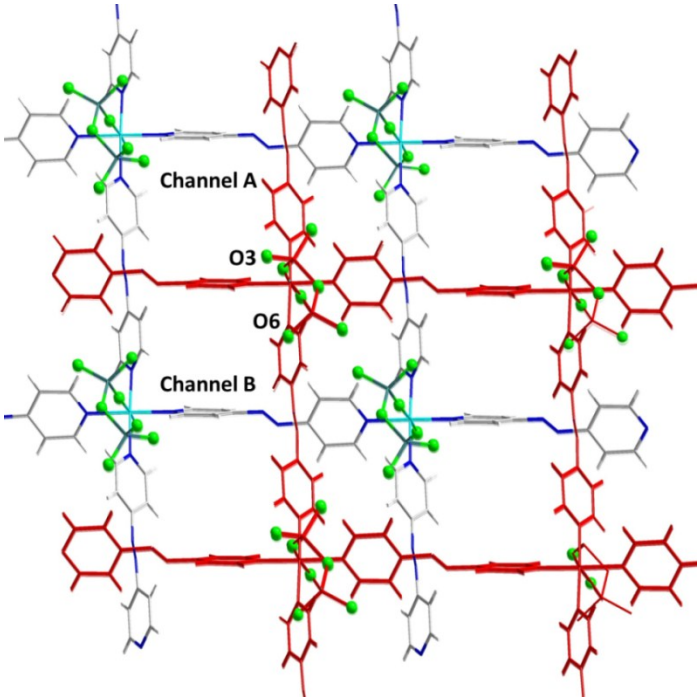

Figure S7. Packing diagram of **DICRO-3-M-i** compounds. Viewed down *a*-axis. One framework is presented red in colour, while the other framework is shown in default atom-based colours to highlight the contrast of the two frameworks. O-atoms are given in light-green in ball-and-stick representation. This view shows the formation of four distinct channels running through the structure.

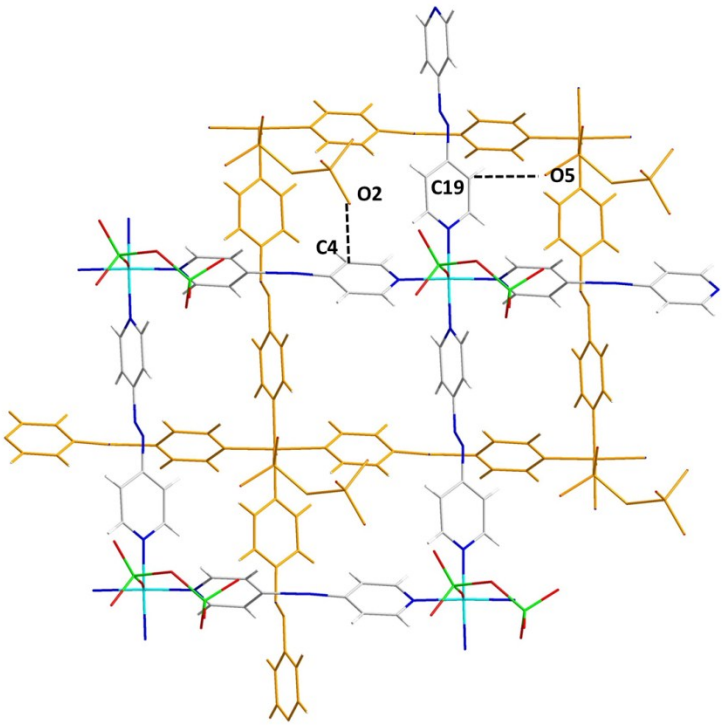

Figure S8. Example of C(H)···O close contacts in **DICRO-3-Cu-i**. Pyridyl groups of one net show C(H)···O contacts to **DICRO** pillar in second framework (C19(H19)…O5 = 3.10 Å and C4(H4)…O2 = 3.22 Å). View down *a*-axis.

Single component gas sorption isotherms

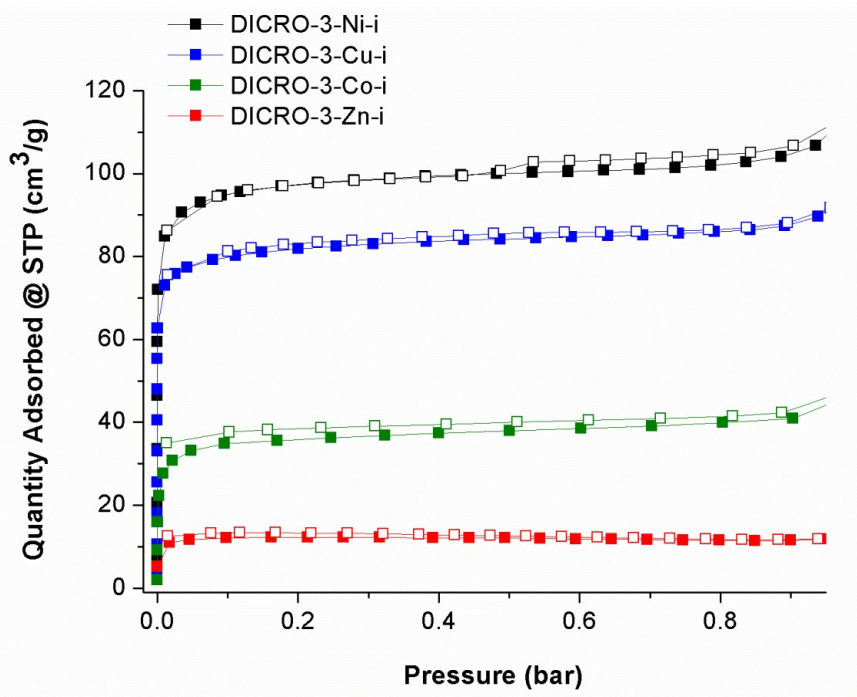

Figure S9. N_2 adsorption isotherms measured at 77 K. Closed symbols = adsorption, open symbols = desorption.

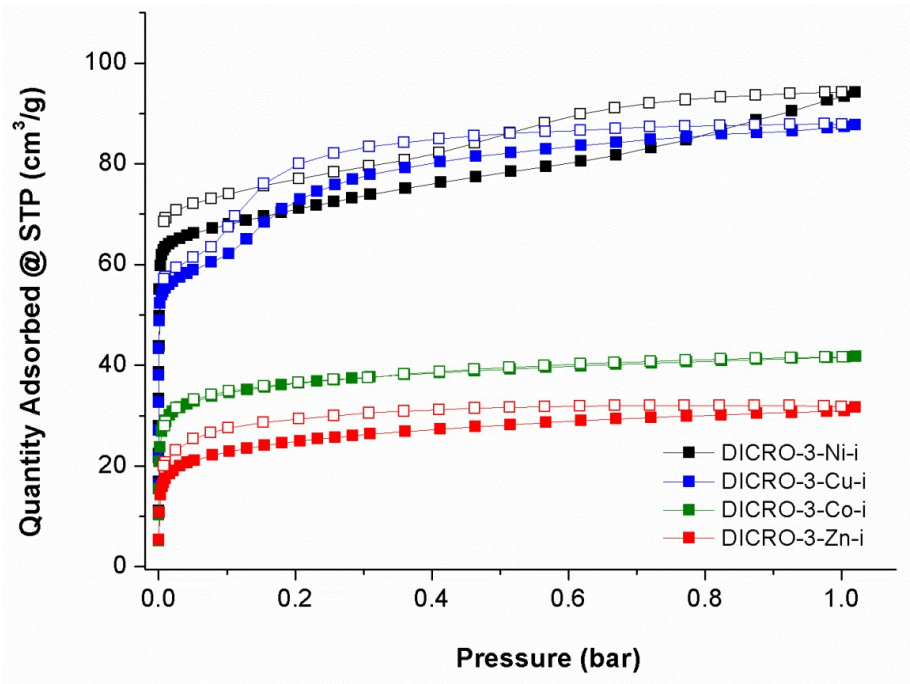

Figure S10. CO_2 adsorption isotherms measured at 195 K. Closed symbols = adsorption, open symbols = desorption.

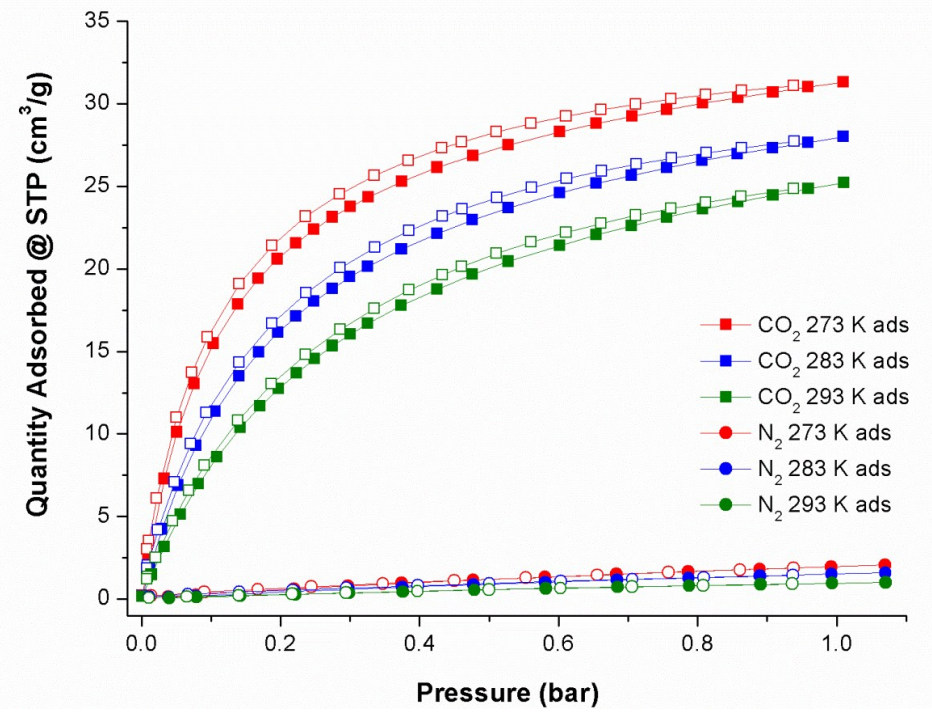

Figure S11. Single component gas sorption isotherms for **DICRO-3-Co-i**. Closed symbols = adsorption, open symbols = desorption.

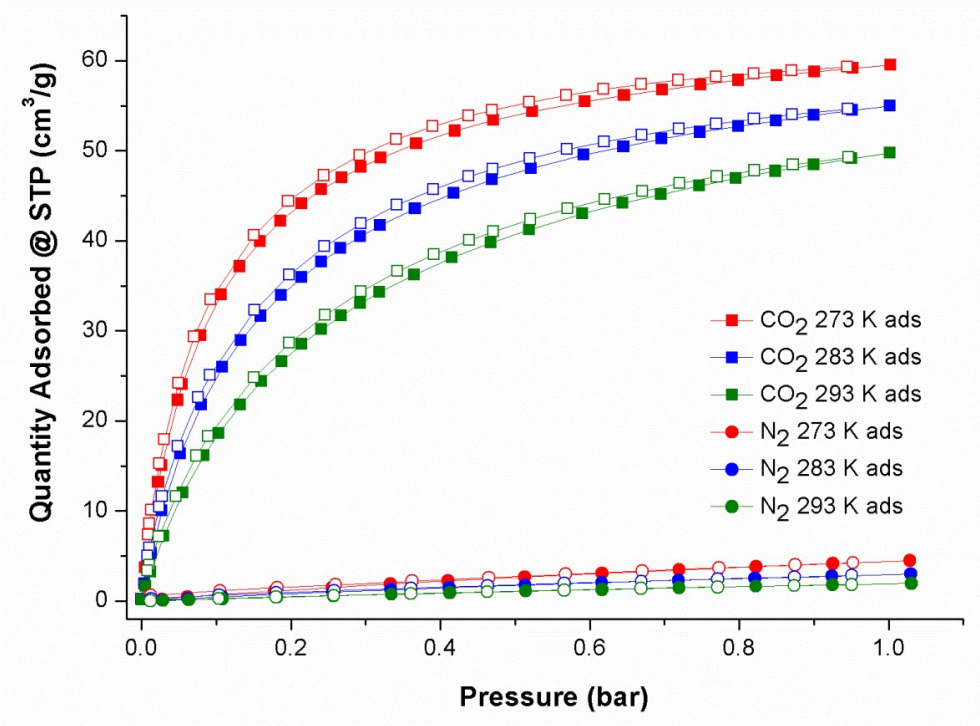

Figure S12. Single component gas sorption isotherms for **DICRO-3-Ni-i**. Closed symbols = adsorption, open symbols = desorption.

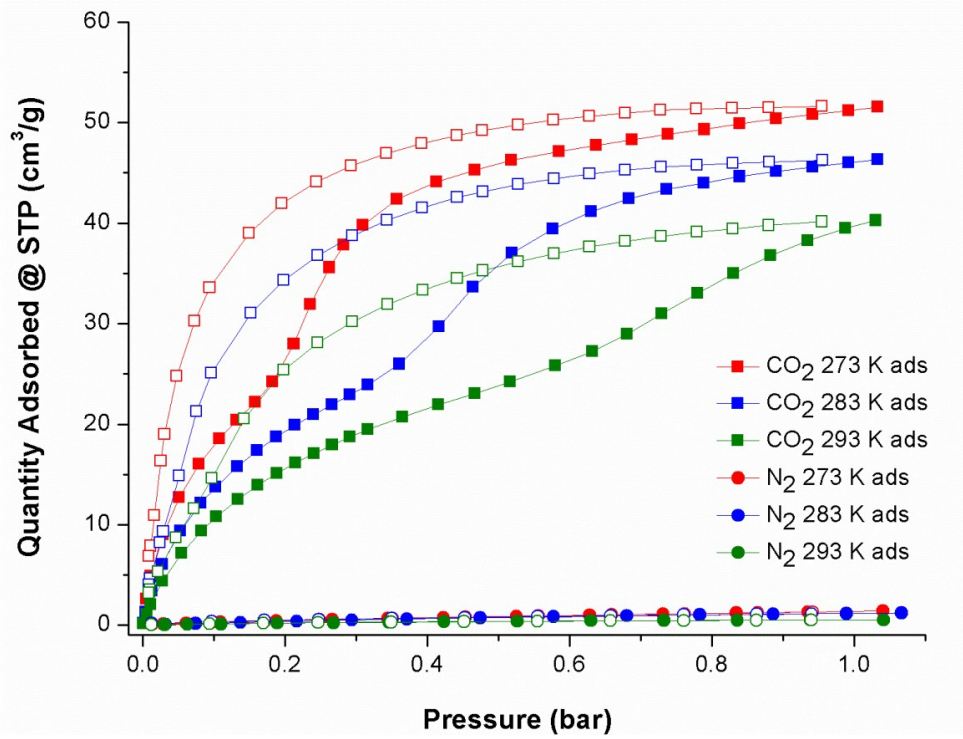

Figure S13. Single component gas sorption isotherms for **DICRO-3-Cu-i**. Closed symbols = adsorption, open symbols = desorption.

Table S3. Total gas uptake (cm^3/g) for **DICRO-3-M-i** compounds.

		DICRO-3-Co-i	DICRO-3-Ni-i	DICRO-3-Cu-i
CO_2	195 K	41.657	94.158	87.730
	273 K	31.322	59.514	51.557
	283 K	28.009	54.972	46.344
	293 K	25.208	49.765	40.260
N_2	77 K	69.157	184.29	142.76
	273 K	2.0545	4.4761	1.4062
	283 K	1.5905	2.9941	1.2120
	293 K	1.0150	1.9503	0.51152

Preliminary selectivity values were calculated at 293 K from single component N_2 and CO_2 data. Langmuir curves were fitted to CO_2 isotherms and used to calculate uptake at pressure of 0.85 bar. Linear curves were fitted to N_2 data and uptake calculated at 0.15 bar.

Variable pressure PXRD

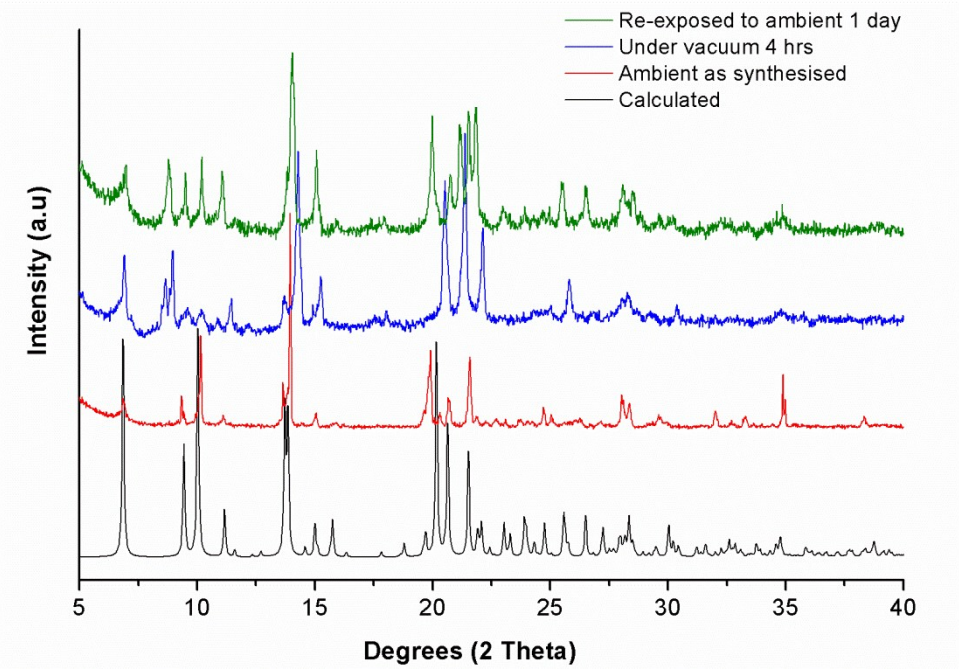

Figure S14. Variable pressure PXRD measurements on **DICRO-3-Cu-i.**

Calculation of isosteric heat of adsorption (Q_{st}) towards CO_2

The Q_{st} value for **DICRO-3-Co-i**, **DICRO-3-Ni-i** and **DICRO-3-Cu-i** were calculated according to the virial equation using the fitted adsorption isotherms at three temperatures (273, 283 and 298 K).

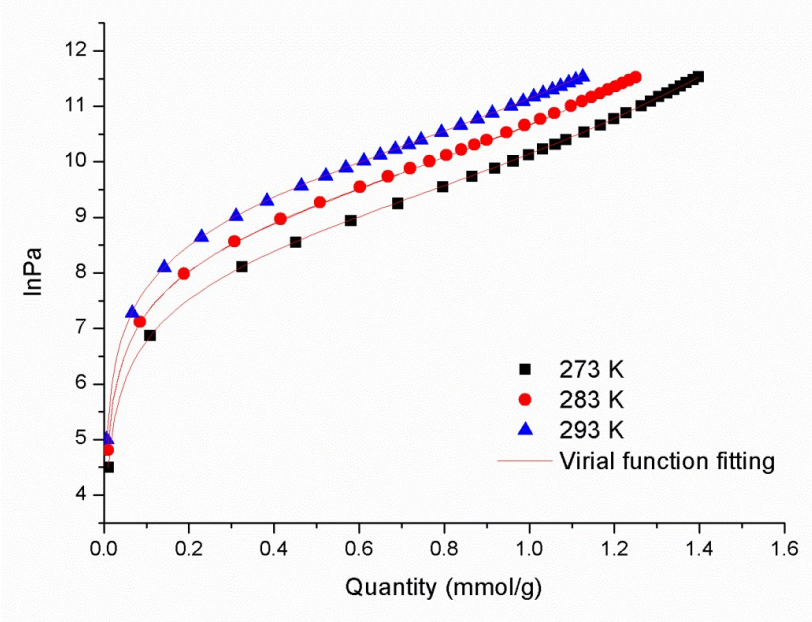

Figure S15. CO_2 adsorption isotherms of **DICRO-3-Co-i** at 273, 283 and 293 K fitted using the virial equation.

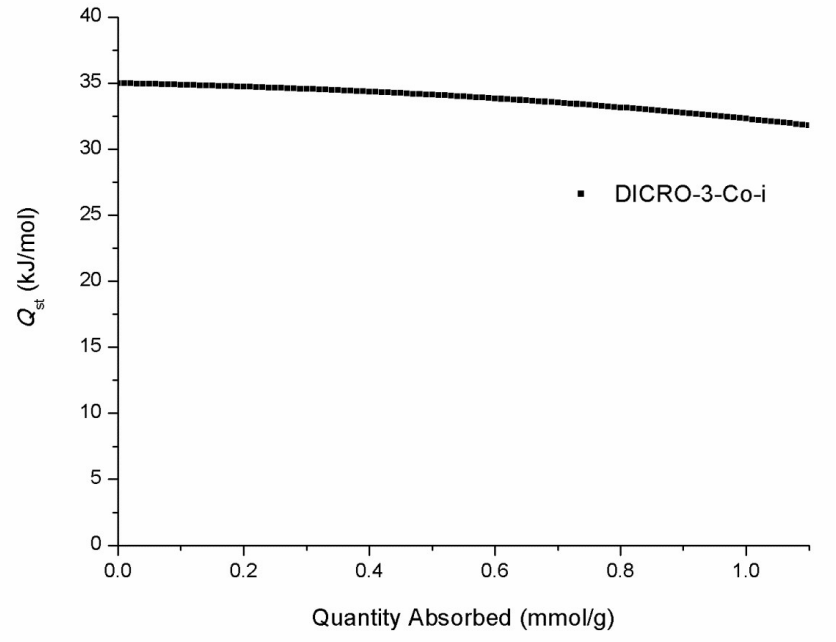

Figure S16. CO_2 isosteric heats of adsorption (Q_{st}) of **DICRO-3-Co-i** using the fitted data measured at 273, 283 and 293 K.

Table S4. Parameters used to fit virial equation for **DICRO-3-Co-i**.

Equation	y = ln(x)+1/T*(a0+a1*x+a2*x^2+a3*x^3+a4*x^4+a5*x^5)+(b0+b1*x+b2*x^2+b3*x^3)			
Adj. R-Square				0.9995
		Value	Standard Error	
A	a0	-4209.34	39.81989	
A	a1	135.7521	51.53234	
A	a2	119.2436	149.48061	
A	a3	78.22709	156.74421	
A	a4	-8.65499	54.21305	
A	a5	0	0	
A	T	273	0	
A	b0	24.39563	0.13957	
A	b1	0	0	
A	b2	0	0	
A	b3	0	0	
D	a0	-4209.34	39.81989	
D	a1	135.7521	51.53234	
D	a2	119.2436	149.48061	
D	a3	78.22709	156.74421	
D	a4	-8.65499	54.21305	
D	a5	0	0	
D	T	273	0	
D	b0	24.39563	0.13957	
D	b1	0	0	
D	b2	0	0	
D	b3	0	0	
F	a0	-4209.34	39.81989	
F	a1	135.7521	51.53234	
F	a2	119.2436	149.48061	
F	a3	78.22709	156.74421	
F	a4	-8.65499	54.21305	
F	a5	0	0	
F	T	273	0	
F	b0	24.39563	0.13957	
F	b1	0	0	
F	b2	0	0	
F	b3	0	0	

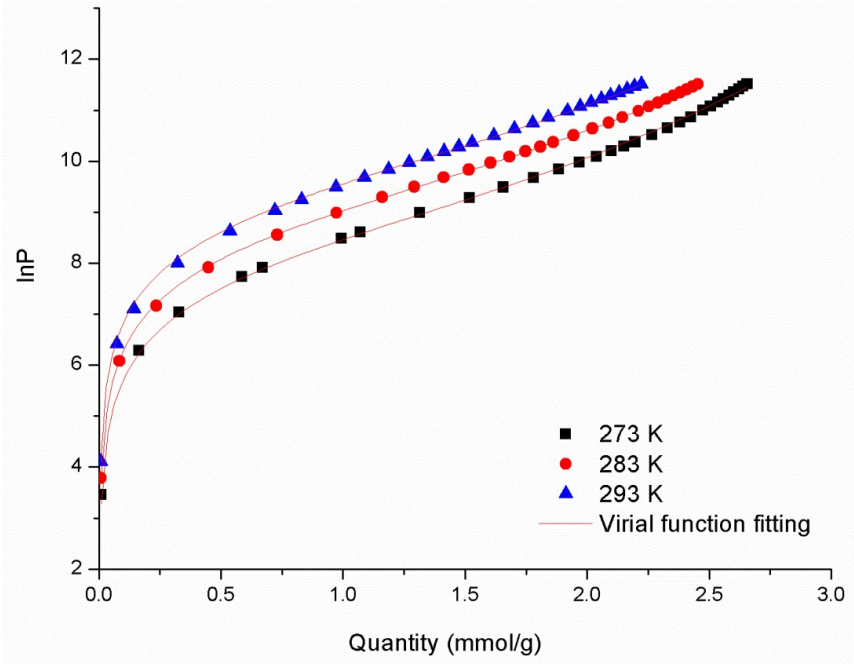

Figure S17. CO_2 adsorption isotherms of **DICRO-3-Ni-i** at 273, 283 and 293 K fitted using the virial equation.

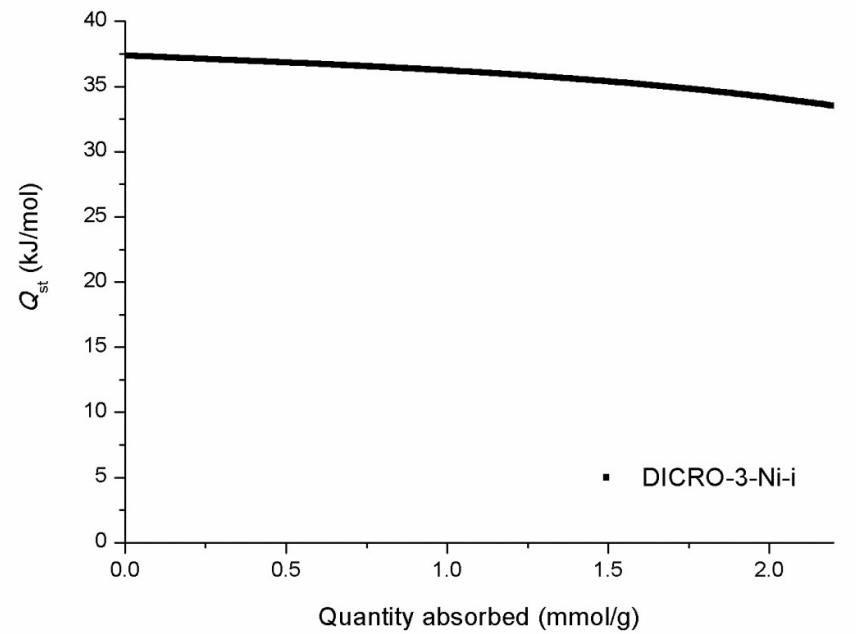

Figure S18. CO_2 isosteric heats of adsorption (Q_{st}) of **DICRO-3-Ni-i** using the fitted data measured at 273, 283 and 293 K.

Table S5. Parameters used to fit virial equation for **DICRO-3-Co-i**.

Equation	y = ln(x)+1/T*(a0+a1*x+a2*x^2+a3*x^3+a4*x^4+a5*x^5)+(b0+b1*x+b2*x^2+b3*x^3)			
Adj. R-Square				0.99945
		Value	Standard Error	
A	a0	-445.901	48.42964	
A	a1	133.9023	16.11047	
A	a2	-22.0448	14.06697	
A	a3	25.99085	3.43025	
A	a4	0	0	
A	a5	0	0	
A	T	273	0	
A	b0	24.42811	0.16934	
A	b1	0	0	
A	b2	0	0	
A	b3	0	0	
D	a0	-445.901	48.42964	
D	a1	133.9023	16.11047	
D	a2	-22.0448	14.06697	
D	a3	25.99085	3.43025	
D	a4	0	0	
D	a5	0	0	
D	T	273	0	
D	b0	24.42811	0.16934	
D	b1	0	0	
D	b2	0	0	
D	b3	0	0	
F	a0	-445.901	48.42964	
F	a1	133.9023	16.11047	
F	a2	-22.0448	14.06697	
F	a3	25.99085	3.43025	
F	a4	0	0	
F	a5	0	0	
F	T	273	0	
F	b0	24.42811	0.16934	
F	b1	0	0	
F	b2	0	0	
F	b3	0	0	

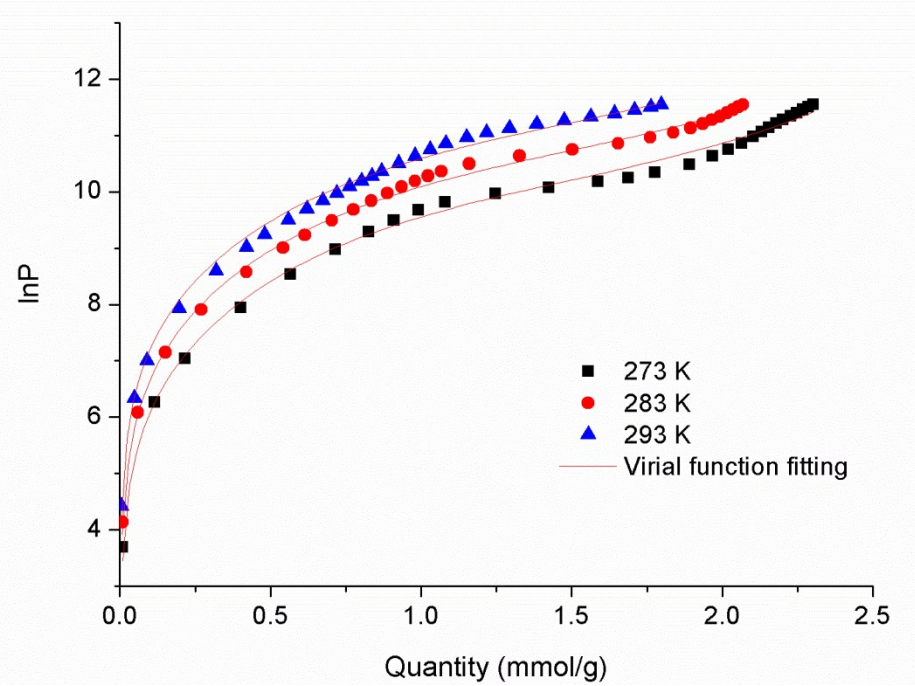

Figure 19 CO_2 adsorption isotherms of **DICRO-3-Cu-i** at 273, 283 and 293 K fitted using the virial equation.

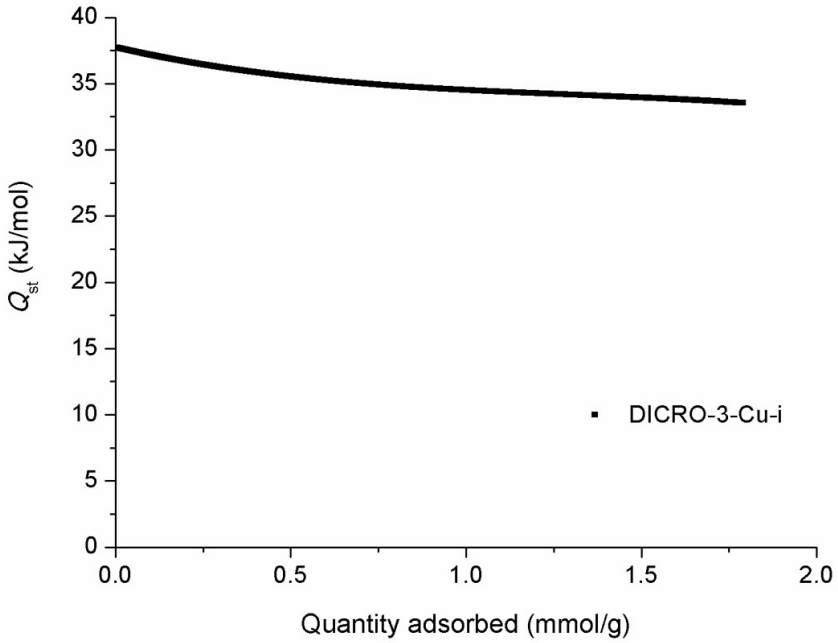

Figure S20. CO_2 isosteric heats of adsorption (Q_{st}) of **DICRO-3-Cu-i** using the fitted data measured at 273, 283 and 293 K.

Table S6. Parameters used to fit virial equation for **DICRO-3-Cu-i**.

Equation	y = ln(x)+1/T*(a0+a1*x+a2*x^2+a3*x^3+a4*x^4+a5*x^5) +(b0+b1*x+b2*x^2+b3*x^3)			
Adj. R-Square				0.99573
		Value	Standard Error	
A	T	273	0	
A	a0	-4540.24	135.4086	
A	a1	730.9366	44.99256	
A	a2	-457.815	47.15087	
A	a3	115.7841	13.7946	
A	a4	0	0	
A	a5	0	0	
A	b0	24.75861	0.47405	
A	b1	0	0	
A	b2	0	0	
A	b3	0	0	
C	T	283	0	
C	a0	-4540.24	135.4086	
C	a1	730.9366	44.99256	
C	a2	-457.815	47.15087	
C	a3	115.7841	13.7946	
C	a4	0	0	
C	a5	0	0	
C	b0	24.75861	0.47405	
C	b1	0	0	
C	b2	0	0	
C	b3	0	0	
E	T	293	0	
E	a0	-4540.24	135.4086	
E	a1	730.9366	44.99256	
E	a2	-457.815	47.15087	
E	a3	115.7841	13.7946	
E	a4	0	0	
E	a5	0	0	
E	b0	24.75861	0.47405	
E	b1	0	0	
E	b2	0	0	
E	b3	0	0	

Molecular simulations

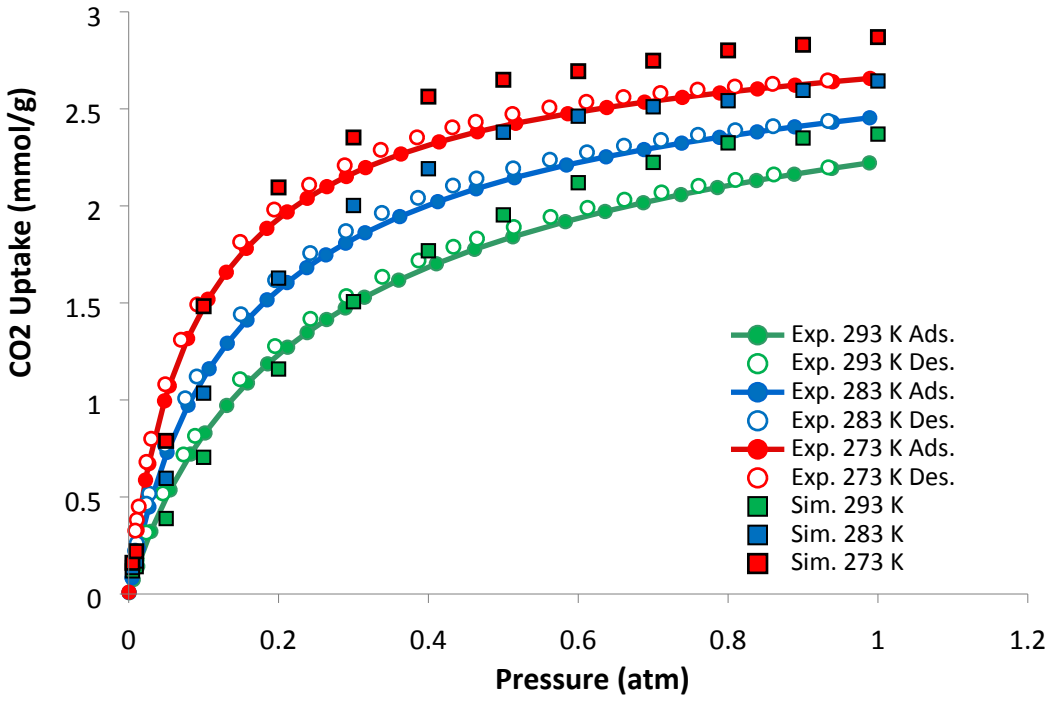

Figure S21. Experimental (lines with circles) and simulated (squares) CO_2 adsorption isotherms in **DICRO-3-Ni-i** at 273 (red), 283 (blue), and 293 K (green).

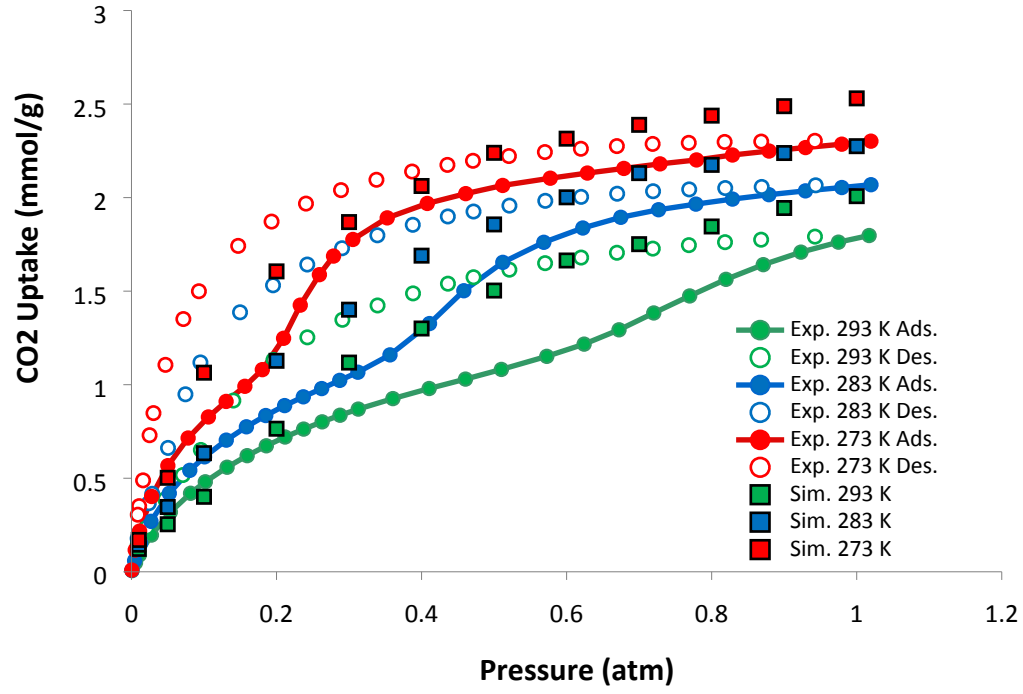

Figure S22. Experimental (lines with circles) and simulated (squares) CO_2 adsorption isotherms in **DICRO-3-Cu-i** at 273 (red), 283 (blue), and 293 K (green).

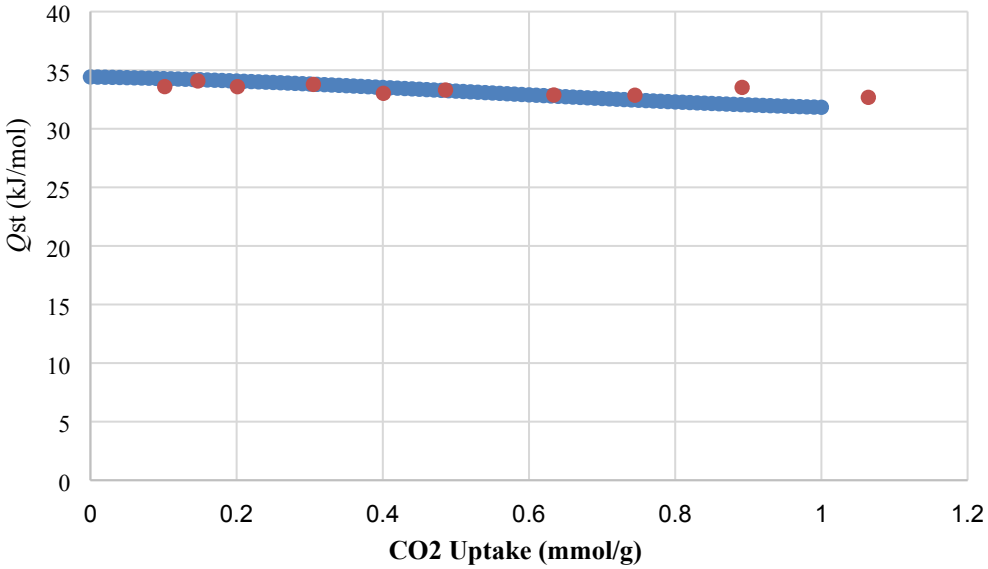

Figure S23. Experimental (blue line) and calculated (red dots) Q_{st} towards **CO_2 DICRO-3-Cu-i.**

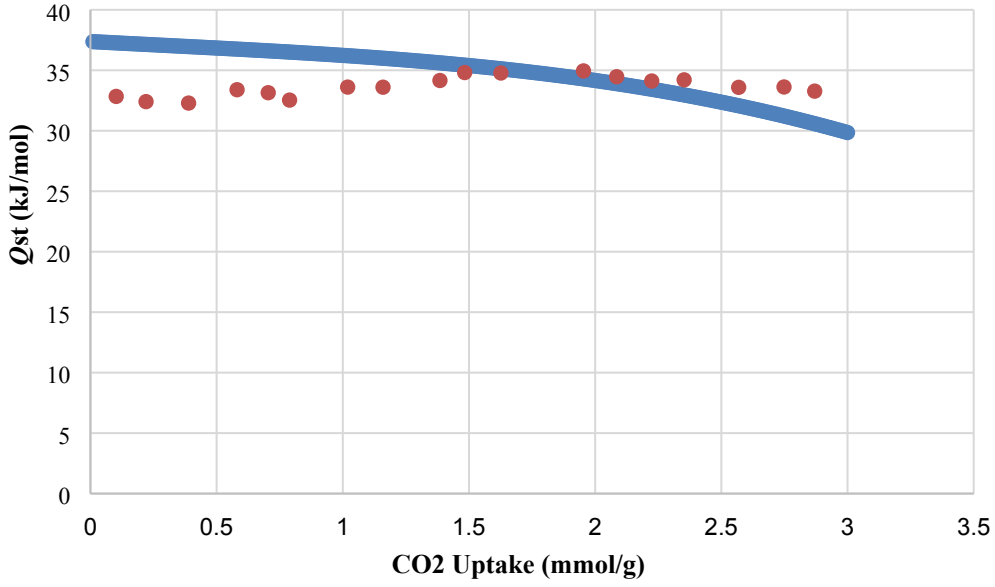

Figure S24. Experimental (blue line) and calculated (red dots) Q_{st} towards CO_2 **for DICRO-3-Ni-i.**

Modeling Details

Simulations of CO_2 adsorption were performed on **DICRO-3-Co-i**, **DICRO-3-Ni-i**, and **DICRO-3-Cu-i** using grand canonical Monte Carlo (GCMC) methods[5] in a 2 × 2 × 2 system cell of the respective MOMs. The single X-ray crystallographic structures that were obtained for all three MOMs herein were used for the parametrisations and simulations. A spherical cut-off distance corresponding to half the shortest system cell dimension length was used for the simulations in all three MOMs. A five-site polarisable potential that was developed previously for CO_2 was used for the simulations in this work.[6] The total potential energy of the MOM–CO_2 system was calculated through the sum of the repulsion/dispersion, electrostatic, and polarisation energies. These were calculated using the Lennard-Jones potential, partial charges with Ewald summation,[7] and a Thole-Applequist type model,[8] respectively. The chemical potential for CO_2 was determined for a range of temperatures through the Peng-Robinson equation of state.[9] All MOM atoms were held fixed throughout the simulations. All simulations were performed using the Massively Parallel Monte Carlo (MPMC) code.[10] For all state points considered, the simulations consisted of 2.5 × 10^6 Monte Carlo steps to guarantee equilibration, followed by an additional 2.5 × 10^6 steps to sample the desired thermodynamic properties.

For all three MOMs, the Lennard-Jones parameters (ε and σ) for all aromatic C, H, and N atoms were taken from the Optimised Potentials For Liquid Simulations – All Atom (OPLS-AA) force field,[11] while such parameters for Ni, Cr, and O were taken from the Universal Force Field (UFF).[12] The partial charges for the chemically distinct atoms in all three **DICRO-3-M-i** variants (Figure S25) were determined through electronic structure calculations on a variety of gas phase fragments that were extracted from the crystal structure of the respective MOMs. For these calculations, all light atoms (C, H, N, and O) and many-electron metal ions (Ni^{2+} and Cr^{6+}) were treated with the 6-31G* and LANL2DZ ECP basis sets,[13] respectively. The NWChem *ab initio* software[14] was used to calculate the electrostatic potential surface for each fragment and the partial charges were subsequently fitted onto the atomic positions of the fragments using the CHELPG method.[15] For each chemically distinct atom, the partial charges were averaged between the fragments. The final partial charges for each chemically distinct atom in **DICRO-3-Co-i**, **DICRO-3-Ni-i**, and **DICRO-3-Cu-i** are provided in Table S7. Note, the crystallographic distances between various chemically distinct atoms for all three MOMs are provided in Table S8. The exponential damping-type atomic point polarisabilities for all C, H, N, and O atoms were taken from a carefully parametrised set provided by the work of van Duijnen and Swart (C = 1.28860 Å^3, H = 0.41380 Å^3, N = 0.97157 Å^3, O = 0.85200 Å^3).[16] The polarisability parameters for Ni^{2+} and Cr^{6+} were determined in previous work (Ni^{2+} = 2.94650 Å^3, Cr^{6+} = 3.50740 Å^3)[17] and were used for the calculations herein. These polarisability values were assigned to the nuclear centers of all atoms of the respective MOMs to model explicit polarisation.

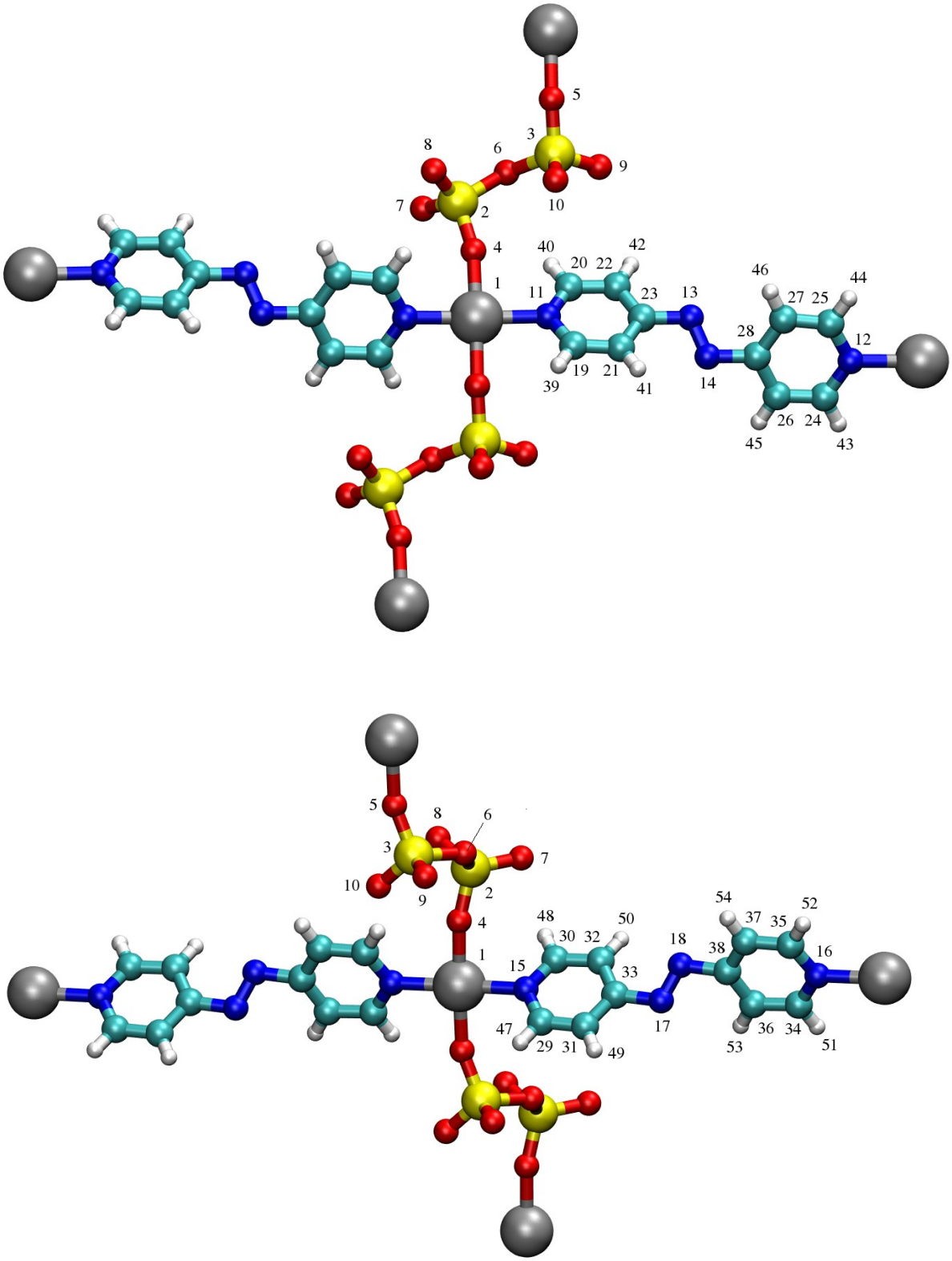

Figure S25. The chemically distinct atoms in **DICRO-3-M-i** (M = Co, Ni, Cu) defining the numbering system corresponding to **Table S7**. Atom colours: C = cyan, H = white, N = blue, O = red, Cr = yellow, Co/Ni/Cu = silver.

Table S7. The partial charges (in e^-) for the chemically distinct atoms in **DICRO-3-M-i** (M = Co, Ni, Cu). Numerical labeling of atoms corresponds to **Figure S25**.

Atom	Label	DICRO-3-Co-i	DICRO-3-Ni-i	DICRO-3-Cu-i
M	1	1.09470	0.45880	0.75020
Cr	2	1.35410	1.26160	1.29980
Cr	3	1.39630	1.32250	1.25080
O	4	–0.79660	–0.60790	–0.72820
O	5	–0.77190	–0.67220	–0.72090
O	6	–0.68980	–0.68950	–0.67590
O	7	–0.61090	–0.61290	–0.63200
O	8	–0.56890	–0.60480	–0.62810
O	9	–0.61820	–0.62360	–0.60850
O	10	–0.60860	–0.58830	–0.62430
N	11	–0.38590	–0.19990	–0.19640
N	12	–0.38850	–0.24260	–0.22240
N	13	–0.23580	–0.27560	–0.23160
N	14	–0.22380	–0.22460	–0.25570
N	15	–0.46520	–0.18100	–0.31660
N	16	–0.48050	–0.14120	–0.30270
N	17	–0.21970	–0.23340	–0.24910
N	18	–0.10970	–0.24930	–0.24600
C	19	0.20270	0.20940	0.20510
C	20	0.32890	0.26700	0.33080
C	21	–0.43870	–0.46010	–0.47770
C	22	–0.58440	–0.54510	–0.52610
C	23	0.57520	0.59850	0.60900
C	24	0.32150	0.31860	0.38850
C	25	0.16650	0.21170	0.26990
C	26	–0.49960	–0.49240	–0.58850
C	27	–0.43240	–0.47020	–0.48670
C	28	0.60070	0.57120	0.63920
C	29	0.31470	0.34520	0.30710
C	30	0.29220	0.23790	0.24240
C	31	–0.51430	–0.59650	–0.52410
C	32	–0.45230	–0.46670	–0.49110
C	33	0.61060	0.63030	0.58290
C	34	0.25780	0.17790	0.27420
C	35	0.35560	0.24400	0.42920
C	36	–0.39130	–0.47780	–0.56230
C	37	–0.49120	–0.53650	–0.72900
C	38	0.59840	0.57990	0.73780
H	39	0.13480	0.13420	0.12990
H	40	0.11430	0.12790	0.14210
H	41	0.20320	0.20220	0.19670
H	42	0.22670	0.22290	0.21340
H	43	0.12120	0.13190	0.11420

H	44	0.11840	0.11740	0.10800
H	45	0.21420	0.20460	0.23190
H	46	0.18000	0.19290	0.17720
H	47	0.11670	0.12180	0.18460
H	48	0.12520	0.12950	0.12970
H	49	0.19360	0.20940	0.21100
H	50	0.17510	0.19080	0.20020
H	51	0.11950	0.14150	0.11520
H	52	0.09140	0.19710	0.10760
H	53	0.17540	0.21560	0.21500
H	54	0.19560	0.21790	0.23030

Table S8. The crystallographic distances (in Å) between various atoms in **DICRO-3-M-i** (M = Co, Ni, Cu). Label of atoms correspond to **Figure S25**.

Atom Pair	DICRO-3-Co-i	DICRO-3-Ni-i	DICRO-3-Cu-i
1–4	2.01190	2.03335	2.34152
1–5	2.02622	2.04606	2.27363
1–11	2.16194	2.10780	2.03679
1–12	2.15085	2.10078	2.04732
1–15	2.19547	2.06801	2.01949
1–16	2.14138	2.08725	2.01870
2–4	1.64393	1.63619	1.61538
2–6	1.76699	1.77795	1.78584
2–7	1.60283	1.59570	1.60048
2–8	1.56169	1.61131	1.60859
3–5	1.62676	1.62880	1.61760
3–6	1.77291	1.77751	1.78357
3–9	1.59720	1.58859	1.60226
3–10	1.59171	1.59196	1.62104
11–19	1.33839	1.34824	1.35208
11–20	1.34480	1.33685	1.33112
12–24	1.34603	1.34873	1.34139
12–25	1.34576	1.34718	1.35059
13–14	1.23579	1.24733	1.24764
13–23	1.41958	1.43394	1.43710
14–28	1.41618	1.43452	1.43870
15–29	1.32673	1.35283	1.34063
15–30	1.28155	1.33856	1.33759
16–34	1.36801	1.33698	1.33532
16–35	1.36449	1.34451	1.35185
17–18	1.19039	1.21886	1.22831
17–33	1.41242	1.43783	1.44612
18–38	1.42975	1.44698	1.43938
19–39	0.95001	0.94975	0.94954
20–40	0.94906	0.95063	0.94945

21–23	1.39589	1.38342	1.38258
21–41	0.95038	0.94934	0.94974
22–23	1.40449	1.37394	1.39335
22–42	0.95152	0.94962	0.95068
24–43	0.94996	0.94979	0.95042
25–44	0.95007	0.95103	0.94997
26–28	1.38933	1.38139	1.38723
26–45	0.95029	0.95069	0.94966
27–28	1.40650	1.39212	1.39052
27–46	0.94925	0.95016	0.94978
29–47	0.95249	0.94917	0.95004
30–48	0.94989	0.94925	0.95032
31–33	1.38578	1.38644	1.37550
31–49	0.95201	0.94970	0.95022
32–33	1.33804	1.39420	1.39220
32–50	0.95090	0.95130	0.94997
34–51	0.95000	0.94961	0.94983
35–52	0.95020	0.94975	0.94977
36–38	1.38999	1.37253	1.38850
36–53	0.94987	0.94942	0.94856
37–38	1.37129	1.35680	1.38399
37–54	0.94991	0.95057	0.94997

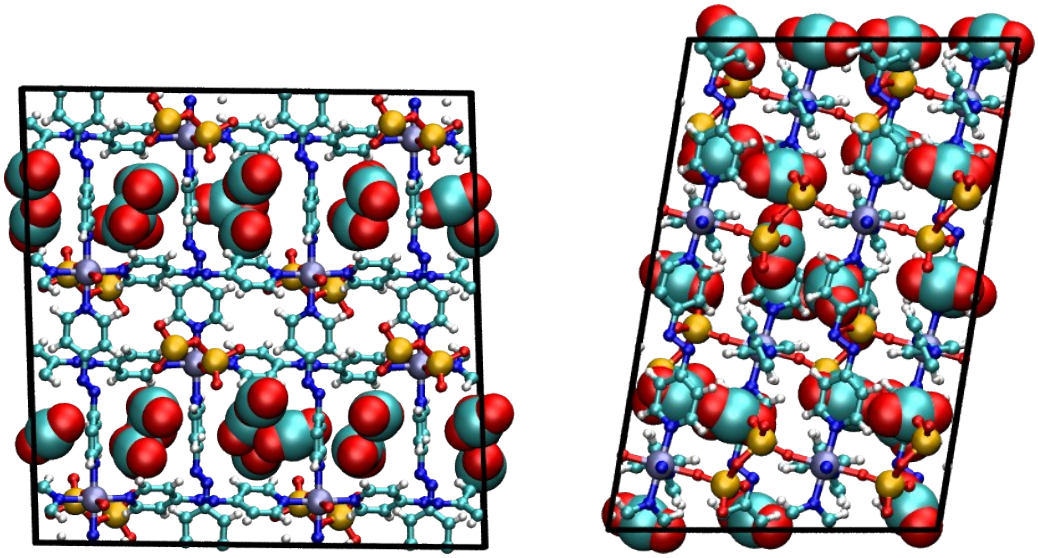

(a) (b)

Figure S26. The *a*-axis view and (b) shifted *c*-axis view of the modeled 2 × 2 × 2 system cell of **DICRO-3-Ni-i** at CO_2 saturation. Atom colors: C = cyan, H = white, N = blue, O = red, Cr = yellow, Ni = lavender.

Stability testing of DICRO-3-Ni-i

Accelerated Stability Protocol. The accelerated stability test was conducted by exposing the samples to 40 °C and 75% relative humidity for a stipulated amount of time in a desiccator. 75% relative humidity was achieved by using a supersaturated aqueous solution of sodium chloride (NaCl) maintained at 40 °C by placing the solution in an enclosed desiccator, which was subsequently placed in an oven held at 40 °C. The time frame used for our studies was 1 day, 7 days and 16 days. Once the sample was subjected to the desired amount of time, it was removed the desiccator and characterised in order to detect if the sample had been affected by exposure to humidity. Characterisation included PXRD, TGA and surface area measurements. For the surface area measurements, the samples were activated under the same degas conditions (same temperature; duration of heating under vacuum) as those used for the pristine compound (see sample preparation sections above).

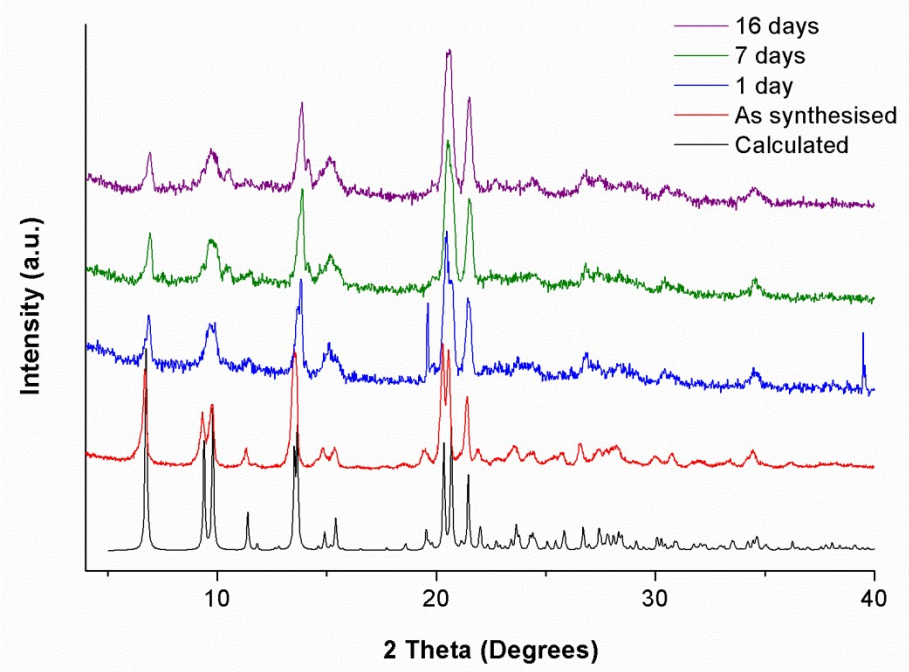

Figure S27. PXRD plots of **DICRO-3-Ni-i** following accelerated stability testing.

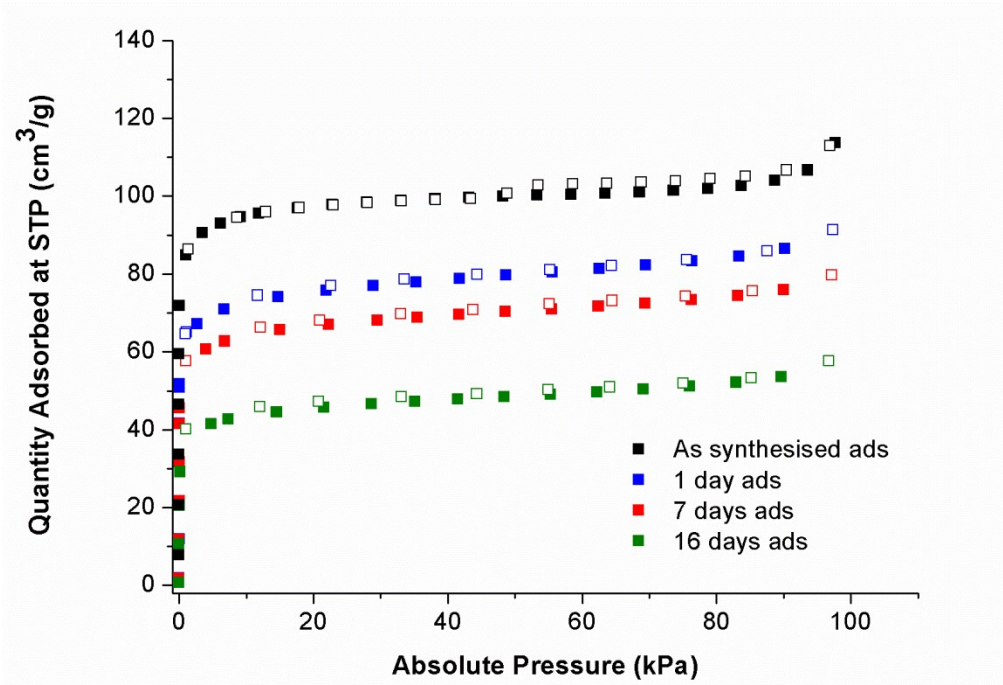

Figure S28. Single component CO_2 isotherms at 293 K of **DICRO-3-Ni-i** following accelerated stability testing.

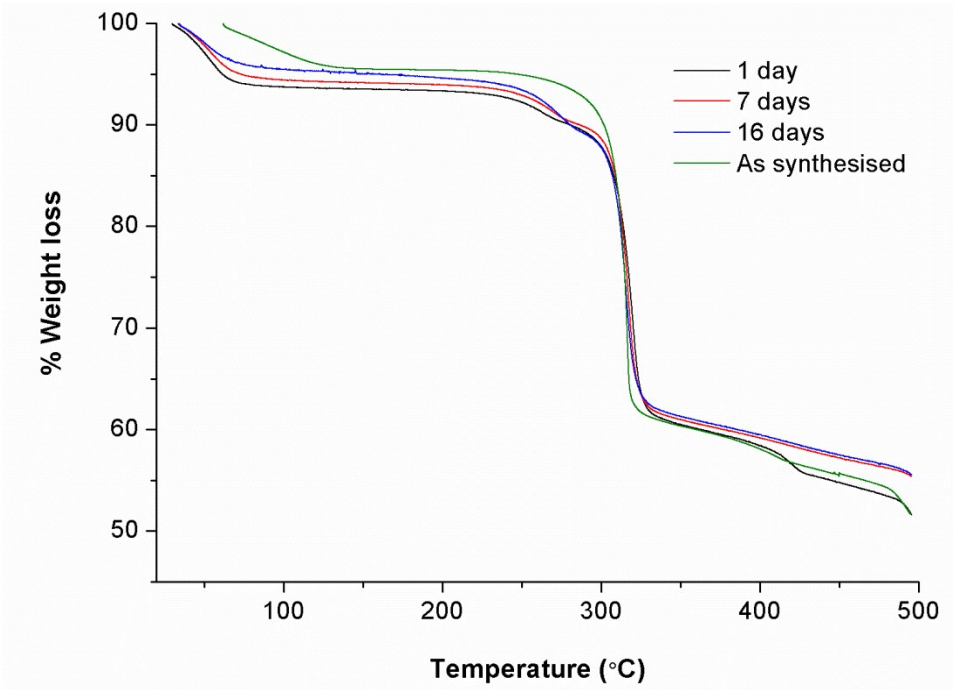

Figure S29. TGA plots of **DICRO-3-Ni-i** following accelerated stability testing.

TGA-Temperature-Programmed Desorption (TPD) of DICRO-3-Ni-i

TGA-TPD studies were carried out on a gas mixing rig coupled independently with a TGA instrument TA Q50 V20.13 Build 39 and mass spectrometer (MS) Agilent 5975 MSD, see Fig. S30. In a typical TGA uptake test the given sample was activated by heating to a desired temperature under a 60 mL/min flow of nitrogen gas. This was then cooled to 30 °C before the chosen gas mixture was introduced to the sample. A mass flow controller was used to control the gas ratios for each test while moisture was introduced by passing the pre-mixed gas through a gas bubbler containing water. The weight increase for each solid was monitored until the weight began to plateau. The exposure time and gas flow conditions were then noted and subsequently applied to samples during TPD studies to analyse the composition of the adsorbed species during the desorption cycle.

TPD tests were carried out using a custom-made fixed-bed flow system. The system consists of a gas delivery system, a reactor housed in a furnace and a mass spectrometer detection system. There are two aims to this testing; to determine the CO_2 adsorbed by the sorbents; to examine the temperatures at which the CO_2 desorption occurs. Both of these parameters will be investigated using CO_2 TPD profiles. In a typical CO_2 TPD cycle, the sorbent is placed in a quartz tubular reactor. The sample is fixed in the reactor using quartz wool. Helium is then passed through the reactor at room temperature until a constant signal is observed using an Agilent 5975 MSD mass spectrometer (MS). The temperature is then increased at a rate of 10 °C/min to an appropriate temperature to remove impurities in the sample. The sample is then cooled to 30 °C. A gas mixture is then introduced to the sorbent for the required length of time. When the required adsorption parameters have been achieved, the gas flow is switched to nitrogen gas until the carbon dioxide concentrations are returned to background levels. The carrier gas is then switched to helium and heated to the required temperature at a rate of 10 °C/min in a flow of helium. The gas composition leaving the reactor is continuously monitored by MS for the identity and quantity of each component of the desorbed gas. Helium is used as a carrier gas as this is not detected by the MS, ensuring that all desorbed species from the adsorbents are detected.

During a direct air capture (DAC) test, a sample is activated under vacuum as per the conditions previously outlined. This sample is then exposed to the laboratory

environment for 24 h. The sample is then analysed using TPD studies to analyse the composition of the exhaust gas from the sorbent.

For calibration, a gas syringe (Valco precision sampling syringe, 2 mL, from Aldrich) was used to introduce pure CO_2, taken directly from a gas cylinder, into the system. Known volumes of CO_2 gas, between 0.2 mL and 5 mL, were injected at a location before the reactor which contained several grams of adsorbent material. The gas flows were continuously monitored using the Agilent 5975 MS. The MS allowed the operator to monitor specific ions continuously throughout the run cycle as well as retrieve complete mass spectra of ions over 12 h for any given time during a test. The material adsorbed all the injected CO_2. Helium gas was allowed to flow through the sample for a further 10 minutes to ensure all the injected CO_2 was adsorbed. If no CO_2 was detected by the MS, the sample was then heated to 200 °C at 10 °C/min while continuously monitoring the level of the desorbed CO_2. The area of the subsequent CO_2 desorption peak was used as a measure of the known volume of injected CO_2. This was repeated several times with different volumes of CO_2 gas. The peak areas associated with the different volumes of injected CO_2 were then used to determine the mass of CO_2 adsorbed in milligrams using the ideal gas law. The culmination of these injections was used to generate a calibration graph seen in Fig. S31. This graph was used to calculate the amount of CO_2 desorbed during a typical TPD run. The H_2O uptake was determined from the overall weight loss/gain observed during gravimetric analysis.

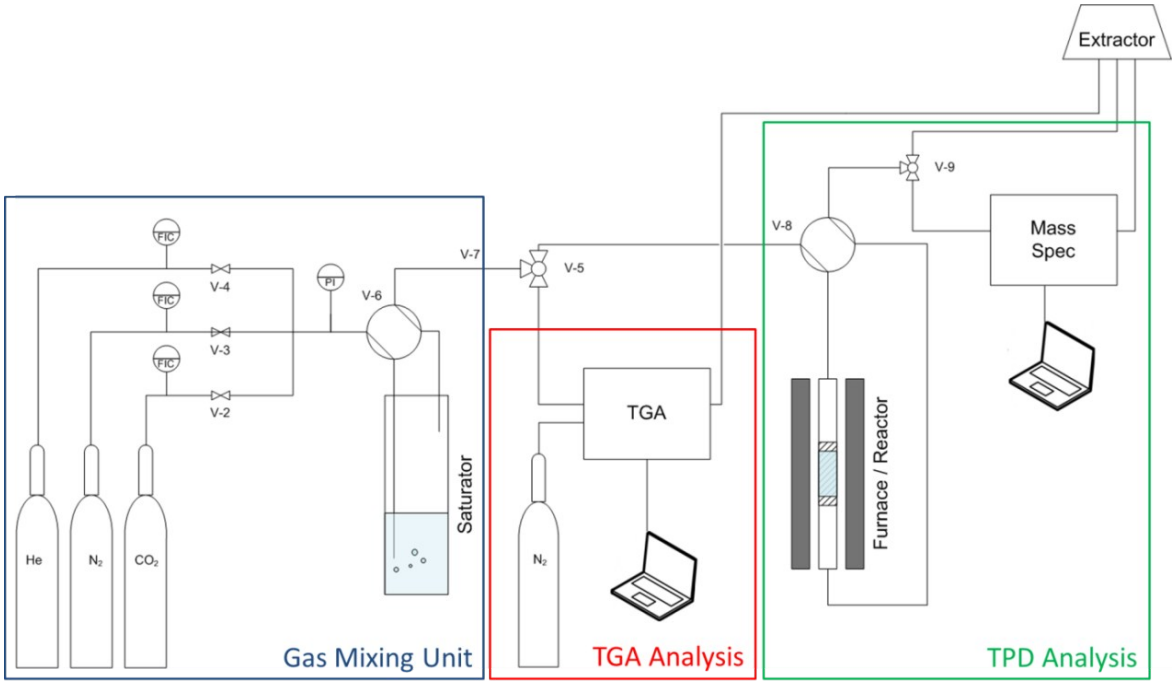

Figure S30. Schematic of gas mixing system, TGA uptake analysis and TPD analysis units.

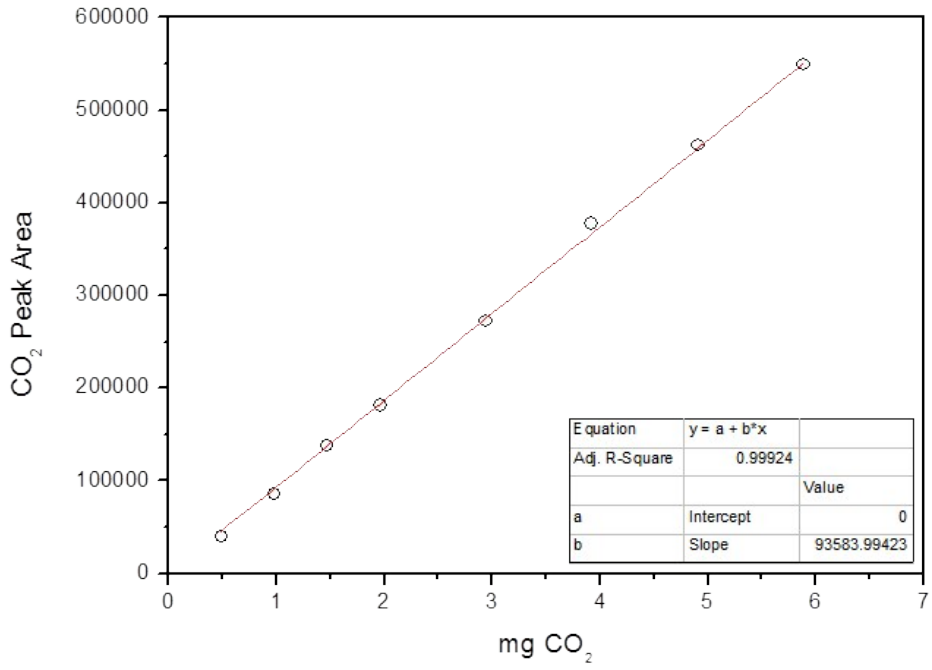

Figure S31. CO_2 calibration graph.

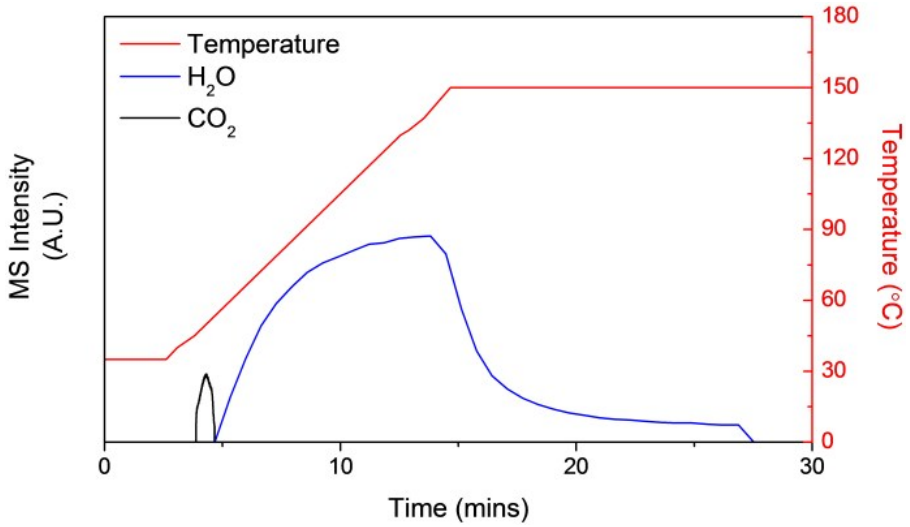

Figure S32. Temperature-Programmed Desorption (TPD) plots of Direct Air Capture (DAC) of CO_2 for **DICRO-3-Ni-i**.

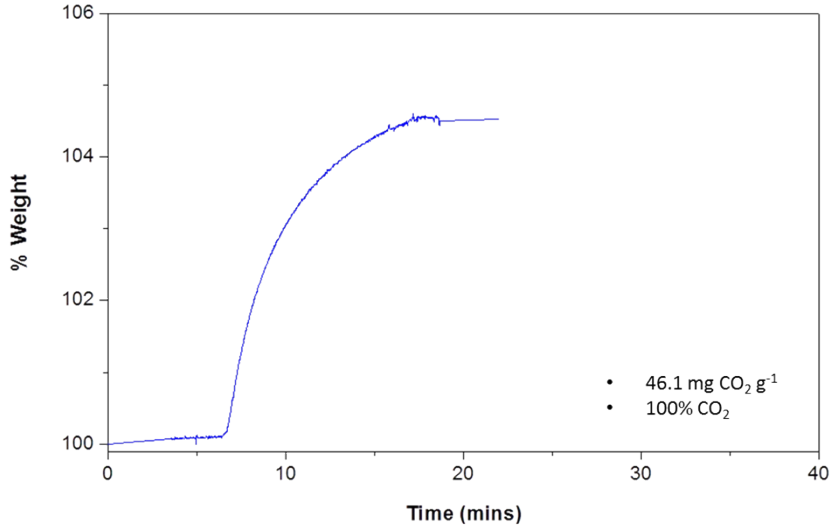

Figure S33. 1.0 atm dry CO_2 uptake, run 1 (35 ˚C). 46.1 mg CO_2/g, 100 % CO_2.

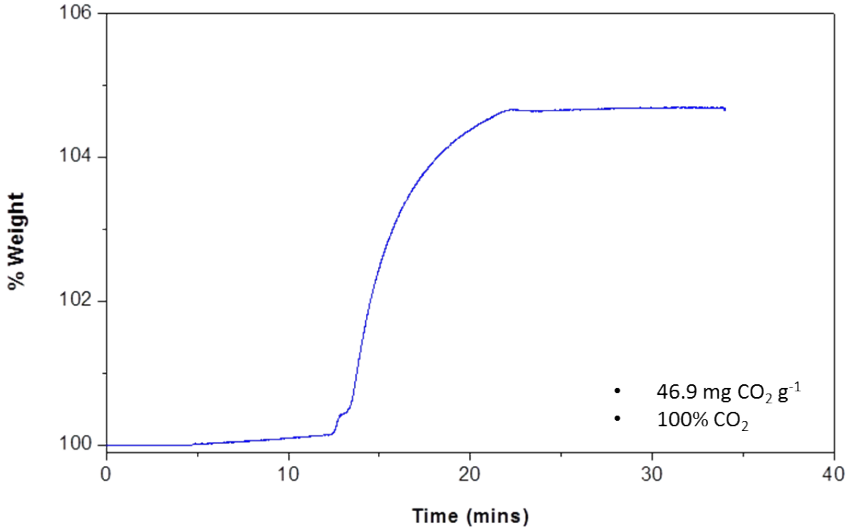

Figure S34. 1.0 atm dry CO_2 uptake, run 2 (+ 5 weeks, 35 ˚C). 46.9 mg CO_2/g, 100 % CO_2.

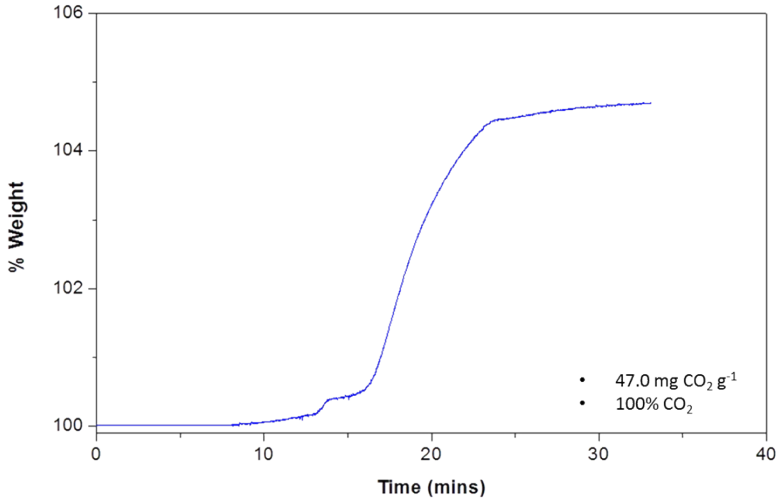

Figure S35. 1.0 atm dry CO_2 uptake, run 3 (+ 6 weeks, 35 ˚C). 47.0 mg CO_2/g, 100 % CO_2.

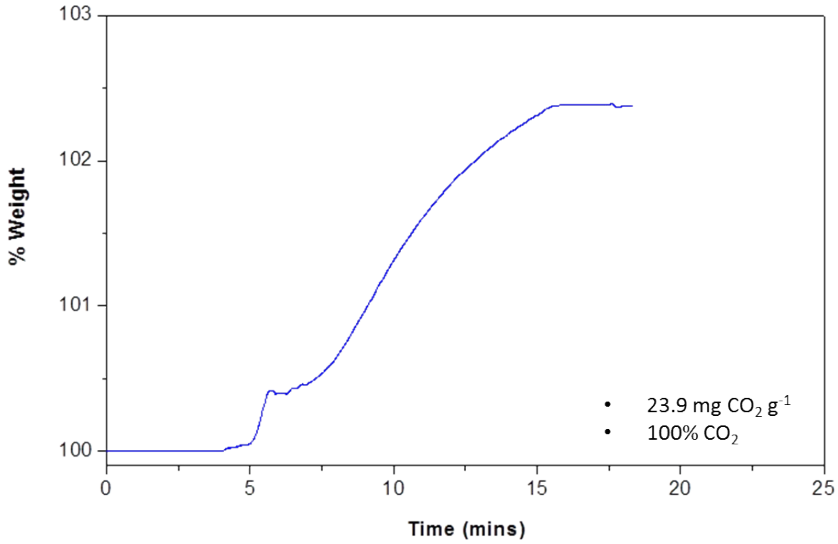

Figure S36. 0.15 atm dry CO_2 uptake. 23.9 mg CO_2/g, 100 % CO_2.

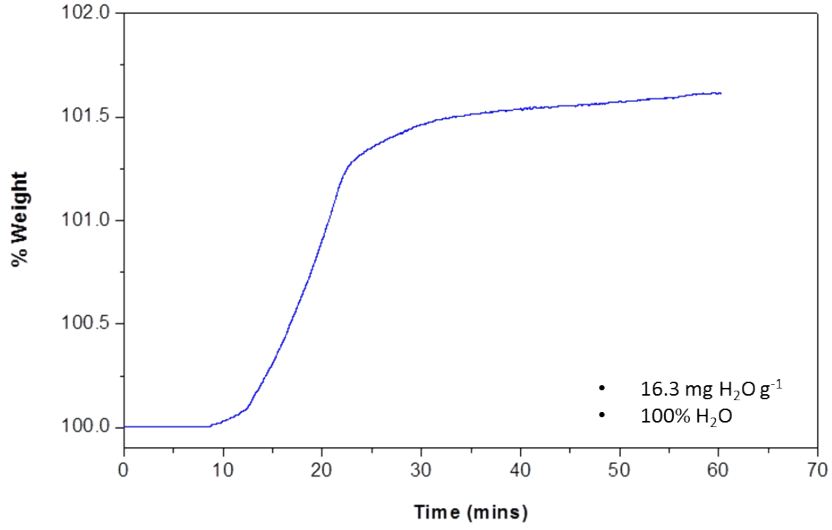

Figure S37. Moist 1.0 atm dry N_2 uptake. 16.3 mg H_2O/g, 100 % H_2O.

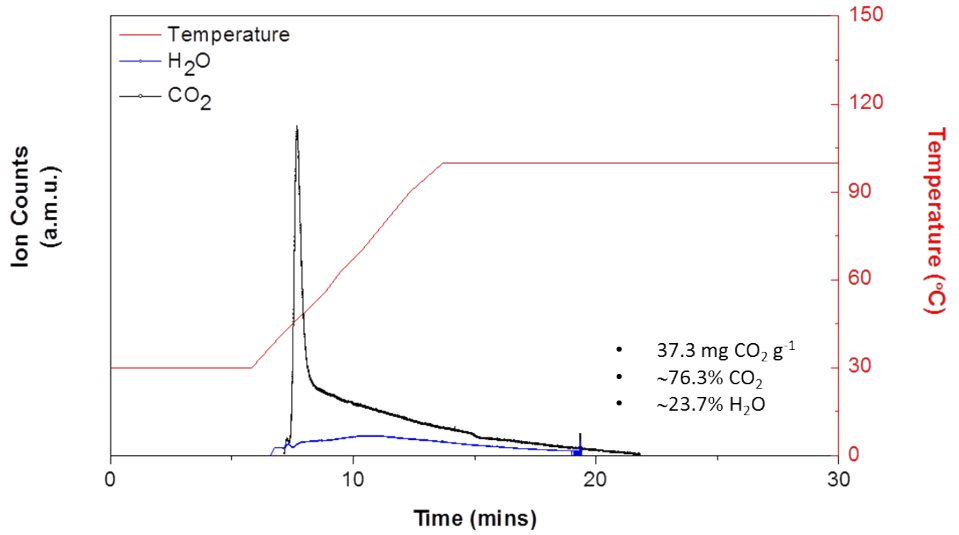

Figure S38. Moist 1.0 atm CO_2 uptake. 37.3 mg CO_2/g, ~76.3% CO_2; ~23.7% H_2O.

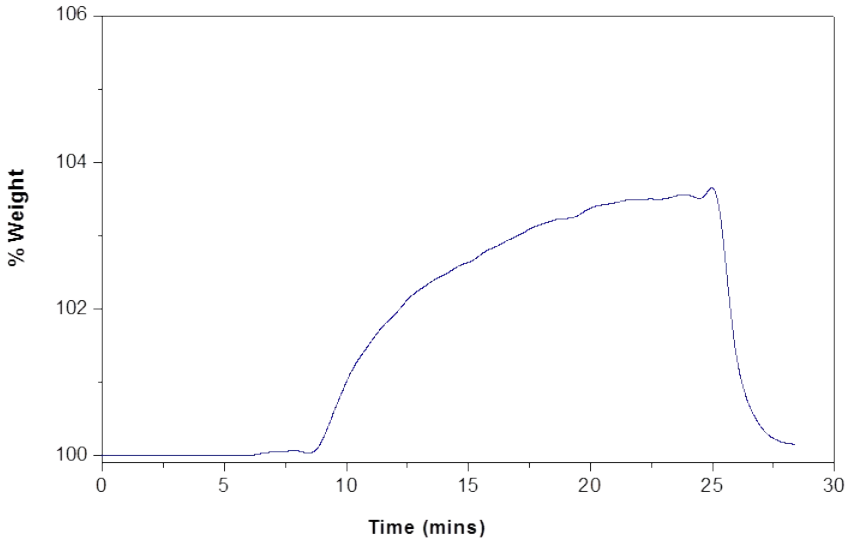

Figure S39. Moist 0.15 atm CO_2.

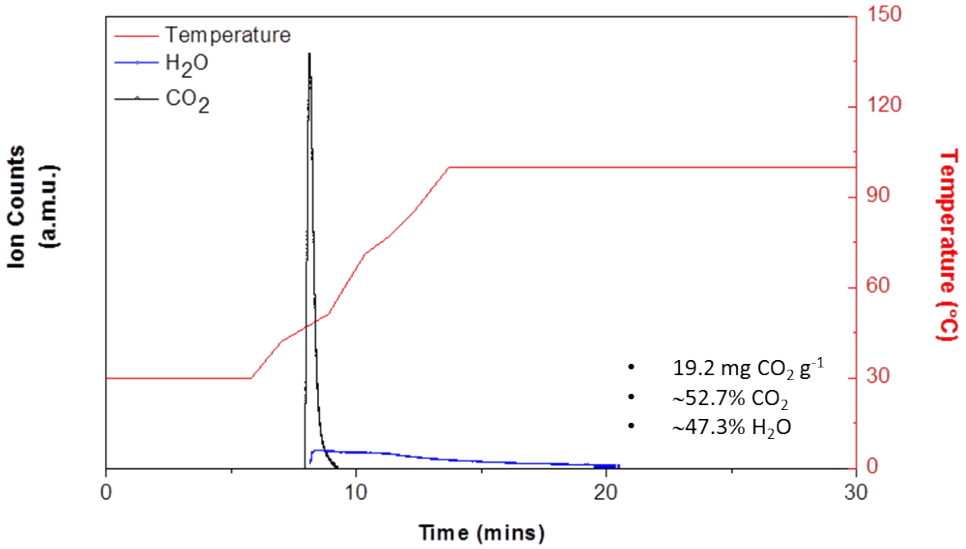

Figure S40. Moist 0.15 atm CO_2, TPD. 19.2 mg CO_2/g. ~52.7% CO_2 ~47.3% H_2O.

Table S9. DAC and TPD uptakes for **DICRO-3-Ni-i**

	DAC (1 atm; 49% RH)			Moist CO_2, (1 atm)			Moist CO_2, (0.15 atm)			Moist N_2 (1 atm)	Dry CO_2 (1 atm)		Dry CO_2 (0.15 atm)	
Sorbent	CO_2	H_2O	CO_2 L/Kg	CO_2	H_2O	CO_2 L/Kg	CO_2	H_2O	CO_2 L/Kg	H_2O	CO_2	CO_2 L/Kg	CO_2	CO_2 L/Kg
DICRO-3-Ni-i	<12% (1.9)	>88% (80)	0.97	>76% (37.3)	<24% (11.6)	18.99	<53% (19.2)	>47% (17.2)	9.77	100% (16.3)	100% (47)	23.93	100% (23.9)	12.17

Values in parentheses below % value indicate mg CO_2 uptake per g sample.

Dynamic Vapour Sorption (DVS)

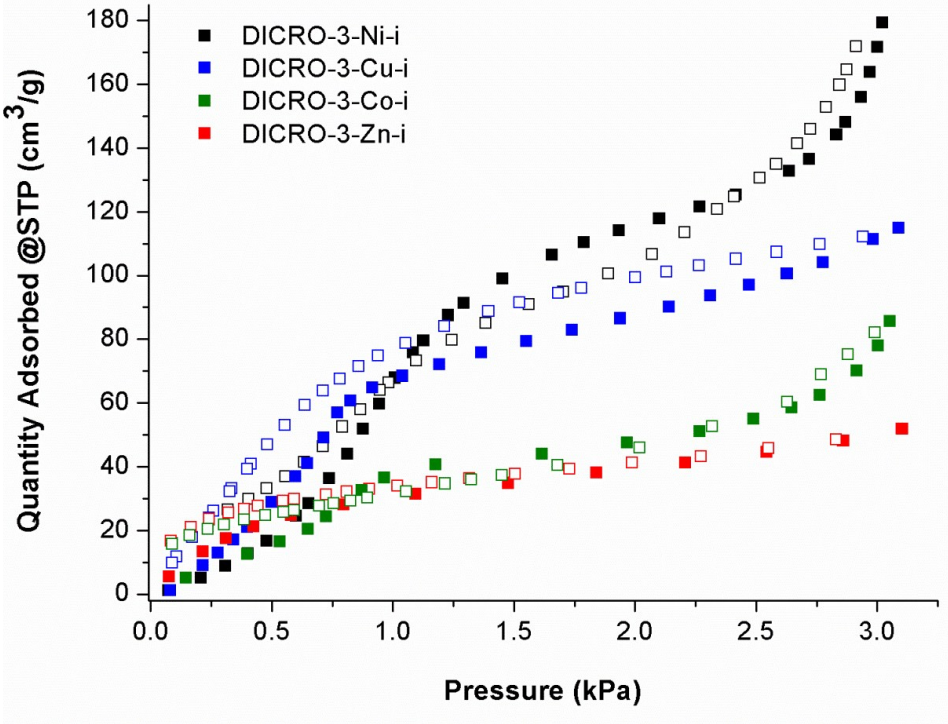

Figure S41. H_2O adsorption isotherms measured at 298 K. Closed symbols = adsorption, open symbols = desorption.

References:

1. Bruker SAINT+, Data Reduction Software, Bruker AXS Inc., Madison, Wisconsin, USA,
2. G. M. Sheldrick, *SADABS*, Program for area detector adsorption correction, Institute for Inorganic Chemistry, Univeristy of Gottingen, Germany, 1996
3. CrystalClear 1.4.0™ d*TREK 9.7 software, Rigaku, Tokyo, Japan,
4. (a). G. M. Sheldrick, *SHELXL-97*, Program for refinement of crystal structures, University of Gottingen, Germany, 1997; (b). A. L. Spek, *Acta Crystallogr. Sect. A*, 1990, **46**, C34.
5. N. Metropolis, A. W. Rosenbluth, M. N. Rosenbluth and A. H. Teller, *J. Chem. Phys.*, 1953, **21**, 1087.
6. A. L. Mullen, T. Pham, K. Forrest, C. R. Cioce, K. McLaughlin and B. Space, *J. Chem. Theory Comput.*, 2013, **9**, 5421.
7. P. P. Ewald, *Ann. Phys.*, 1921, **369**, 253.
8. (a). J. Applequist, J. R. Carl and K.-K. Fung, *J. Am. Chem. Soc.*, 1972, **94**, 2952; (b). K. A. Bode and J. Applequist, *J. Phys. Chem.*, 1996, **100**, 17820; (c). K. McLaughlin, C. R. Cioce, T. Pham, J. L. Belof and B. Space, *J. Phys. Chem.*, 2013, **139**, 184112; (d). B. Thole, *Chem. Phys.*, 1981, **59**, 341.
9. D.-Y. Peng and D. B. Robinson, *Ind. Eng. Chem. Fundam.*, 1976, **15**, 59.
10. https://github.com/mpmccode/mpmc: J. L. Belof and B. Space, 2012.
11. W. L. Jorgensen, D. S. Maxwell and J. Tirado-Rivers, *J. Am. Chem. Soc.*, 1996, **118**, 11225.
12. A. K. Rappe, C. J. Casewit, K. S. Colwell, W. A. Goddard and W. M. Skiff, 1992, **114**, 10024.
13. (a). P. J. Hay and W. R. Wadt, *J. Chem. Phys.*, 1985, **82**, 270; (b). L. A. LaJohn, P. A. Christiansen, R. B. Ross, T. Atashroo and W. C. Ermler, *J. Chem. Phys.*, 1987, **87**, 2812; (c). W. J. Stevens, H. Basch and M. Krauss, *J. Chem. Phys.*, 1984, **81**, 6026.
14. M. Valiev, E. Bylaska, N. Govind, K. Kowalski, T. Straatsma, H. V. Dam, D. Wang, J. Nieplocha, E. Apra, T. Windus and W. de Jong, *Comput. Phys. Commun.*, 2010, **181**, 1477.
15. C. M. Breneman and K. B. Wiberg, *J. Comput. Chem.*, 1990, **11**, 361; L. E. Chirlian and M. M. Francl, *J. Comput. Chem.*, 1987, **8**, 894.
16. P. T. van Duijnen and M. Swart, *J. Phys. Chem. A*, 1998, **102**, 2399.
17. H. S. Scott, A. Bajpai, K. J. Chen, T. Pham, B. Space, J. J. Perry IV and M. Zaworotko, *Chem. Commun.*, 2015, **51**, 14832.